COUPLED-WAVEGUIDE FABRY-PEROT RESONATOR

by

Cheng-Chun Chang

Thesis submitted to the Faculty of the

Viginia Polytechnic Institute and State University

in partial fulfillment of the requirements for the degree of

MASTER OF SCIENCE

in

Electrical Engineering

APPROVED:

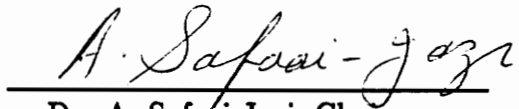

Dr. A. Safaai-Jazi, Chairman

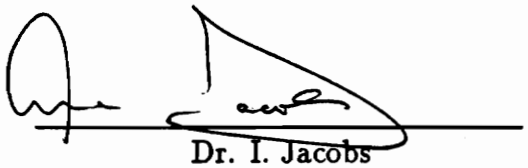

Dr. I. Jacobs

Dr. T. C. Poon

December 1992

Blacksburg, Virginia

C.2

LD
5655
V855
1992
C523
C.2

Coupled-Waveguide Fabry-Perot Resonator

by

Cheng-Chun Chang

Committee Chairman: A. Safaai-Jazi

Electrical Engineering

(ABSTRACT)

Narrowband spectral filters find important applications in optical fiber communication systems, particularly in wavelength demultiplexers and single-frequency semiconductor lasers. Conventional Fabry-Perot resonators provide a narrow spectral width but lack the capability of mode discrimination. A new coupled-waveguide Fabry-Perot resonator made of two parallel waveguides with reflecting mirrors at the ends is proposed for application as narrowband tuned spectral filter in single-mode diode lasers and wavelength demultiplexers.

The interference of counter propagating waves from reflection by end mirrors and the coupling of waves between the two parallel guides contribute to the operation of this resonator structure. Thus, the device exhibits the attributes of both Fabry-Perot resonator and directional coupler. The coupled-mode theory of parallel waveguides is employed to analyze the proposed structure. Spectral characteristics are derived from the governing coupled-mode equations and related boundary conditions.

Two geometries consisting of identical waveguides as well as nonidentical waveguides are examined. The spectral characteristics of the proposed resonator demonstrate that significant improvement in mode discrimination capability and longitudinal mode spacing over the conventional Fabry-Perot resonator is achieved. Numerical results for several example cases are presented and the influence of various parameters on spectral properties are investigated.

Acknowledgements

I wish to express sincere gratefulness and respect to my advisor, Dr. A.Safaai-Jazi, for his ceaseless encouragement, support and guidance throughout the course of this thesis. I would also like to extend my appreciation to the other committee members, Dr. I. Jacobs and Dr. T. C. Poon.

Appreciation also goes to T. S. Chang, T. H. Hsu, and S. Yan for their assistance and friendship.

Lastly, I wish to express my deepest gratitude to my parents for their love, understanding and support in all these years. I dedicate this work to them.

Table of Contents

List of Figures

Chapter 1

Introduction

Narrowband optical filters are of considerable interest in fiber-optic communication systems. These filters find applications in wavelength division multiplexing, single-mode semiconductor lasers, optical spectrum analyzers, Raman light amplifiers, etc. Several types of such filters are more widely used in lightwave systems, including Fabry-Perot resonator, interference filter, grating reflector, and wavelength selective directional coupler. Here, attention is focused on Fabry-Perot resonator and its role in semiconductor diode lasers.

In conventional Fabry-Perot resonators, feedback is provided by facet reflections resulting in longitudinal modes of equal magnitude. Supporting many longitudinal modes, the Fabry-Perot resonator has a limited use as a wavelength selective filter. When used as a cavity resonator in diode lasers, the longitudinal-mode discrimination is provided only by the gain spectrum of the active region. However, since the gain spectrum is usually much wider than the mode spacing, the resulting mode discrimination is poor. Therefore, a single cavity Fabry-Perot diode laser is, strictly speaking, a multimode laser, unless the cavity length is sufficiently short such that

the mode spacing is wider than the gain spectrum. Such short cavity are generally not practical.

To improve the mode selectivity of laser diodes, several types of optical resonators have been developed. The multiple cavity Fabry-Perot resonator, formed by connecting two or more single cavities in tandem or by adding one or more mirrors to a conventional two-mirror cavity, significantly enhances the filtering capability in terms of linewidth and tuning range. In the distributed-feedback (DFB) lasers [1], the optical feedback, instead of being localized at the end mirrors, is distributed throughout the cavity by using Bragg grating reflectors. Mode selectivity in DFB lasers results from the Bragg condition. Both multiple cavity and DFB grating can be used to realize single-frequency diode lasers with a high degree of side-mode suppression and wavelength stability.

In this thesis, a coupled-waveguide Fabry-Perot resonator is proposed. This resonator structure consists of two parallel lightguides with partially reflecting mirrors at the ends. Each guide in isolation can be regarded as a single cavity Fabry-Perot etalon. When the two guides are placed close to each other, the lightwave in each guide not only travels back and forth but also interacts with the lightwave in the other guide. Thus, this device incorporates the features of both Fabry-Perot etalon and directional coupler. The proposed resonator offers a better mode discrimination capability and a narrower spectral width than the conventional Fabry-Perot resonator.

The next three chapters present a literature review and basic concepts upon which the proposed device is based. In Chapter 2, the formulation of coupled-mode theory with application to parallel-waveguide structures is reviewed. Chapter 3 explores the solutions of the coupled-mode equations with particular emphasis on the operation

of directional couplers. The characteristics of conventional two-mirror Fabry-Perot etalons are discussed in Chapter 4. Improvements resulting from the two-cavity Fabry-Perot structure are also discussed in this chapter. In Chapter 5, the proposed couple-waveguide Fabry-Perot resonator is analyzed using the coupled-mode theory of parallel guides. The spectral characteristic of the device is derived from the coupled-mode equations and related boundary conditions. Spectral properties of the proposed device are compared with those of the single cavity Fabry-Perot etalon and the directional coupler. Numerical results are presented in Chapter 6. The effects of parameters on the spectral characteristics of the proposed device are investigated. Concluding remarks and suggestions for future work are summarized in Chapter 7.

Chapter 2

Coupled-Mode Theory

Mode coupling phenomena occur in many physics and engineering problems. Examples of mode coupling can be found in nonlinear optical interactions, acoustooptic and electrooptic switching and modulation, and optical filtering and reflection by periodic structures [3]. The theory of mode coupling was first developed by Pierce [2] to analyze the energy exchange between electron beams and slow-wave structures in electron-beam tubes. Later, a coupled-mode formalism was established for the analysis of optical waveguides [6,9]. In the following sections, we will first briefly review the general coupled-mode formalism [8] which is applicable to the analysis of a large variety of coupled-wave phenomena. This formalism is then used to analyze mode coupling between two parallel waveguides which has long been a subject of considerable interest in the fields of integrated optics and fiber optics.

2.1 General Coupled-Mode Formalism

The Lorentz reciprocity relation derived from Maxwell's equations can be shown to have the integral form [8]

$$\int\int_S dxdy \frac{\partial}{\partial z}(\vec{E}_1 \times \vec{H}_2^* + \vec{E}_2^* \times \vec{H}_1)_z = -j\omega \int\int_S dxdy \vec{P}_1 \cdot \vec{E}_2^*, \tag{2.1}$$

where $(\vec{E}_1, \vec{H}_1)$ and $(\vec{E}_2, \vec{H}_2)$ are two sets of electromagnetic fields, $\vec{P}_1$ is a polarization vector corresponding to field 1, and S is a $z = constant$ plane. In waveguide structures, field 1 may be considered as an unknown field of interest whose transverse components can be expanded in terms of the normal modes (generally, eigenfunctions in boundary value problems) determined by the waveguide structure and its boundary conditions as [8]

$$\vec{E}_{1t} = \sum [a_m(z) + a_{-m}(z)]\, \vec{e}_{mt} = \sum \left[A_m\, e^{-j\beta_m z} + A_{-m}\, e^{j\beta_m z}\right] \vec{e}_{mt} \tag{2.2}$$

$$\vec{H}_{1t} = \sum [a_m(z) - a_{-m}(z)]\, \vec{h}_{mt} = \sum \left[A_m\, e^{-j\beta_m z} - A_{-m}\, e^{j\beta_m z}\right] \vec{h}_{mt} \tag{2.3}$$

where the Σ notation indicates summation over the discrete and finite set of guided modes and integration over the continuous spectrum of radiation modes. If interest is primarily in perturbations which cause coupling only between guided modes, the radiation modes can be dropped from the expansions. The coefficients A_m and A_{-m} in general vary along the waveguide and are functions of z. Substituting equations (2.2) and (2.3) into equation (2.1) and considering field 2 as an n-th forward traveling mode, with the help of orthogonality relations for guided modes we obtain [8]

$$\frac{da_n(z)}{dz} + j\beta_n a_n(z) = -j\omega \int\int_S dxdy \vec{P}_1 \cdot \vec{E}_2^*, \tag{2.4}$$

or in terms of A_n,

$$\frac{dA_n(z)}{dz} = -j\omega \int\int_S dxdy \vec{P}_1 \cdot \vec{E}_2^* \exp(j\beta_n z). \tag{2.5}$$

The polarization $\vec{P}_1$ represents perturbations in a canonical structure and is considered to be a distribution of excitation source. Equation (2.5) can be used to treat various mode interactions. Each physical effect brings about, in general, a different

perturbation polarization but leads to the same set of coupled first-order differential equations called *coupled-wave* or *coupled-mode* equations of the form given in equations (2.7) and (2.8). Yariv [3] has studied several coupled-wave phenomena occurring in integrated optics using this formulation. A well known example of the perturbation polarization is that resulting from a scalar deformation of waveguides

$$\vec{P} = \Delta\varepsilon(x, y, z)\, \vec{E}, \tag{2.6}$$

where $\Delta\varepsilon(x, y, z)$ represents a purterbation in the refractive index of the waveguide. In many coupled-mode interactions of interests, there are only two guided modes that have sufficient phase synchronism to allow for a significant exchange of energy. In such cases, one can neglect all other modes and equation (2.4) can be reduced to a set of coupled-mode equations relating the amplitudes A $(=A_1)$ and B $(=A_2)$ of the two significant modes with the following results

$$\frac{dA(z)}{dz} = -jk_{12}B(z)\exp(2j\delta z) \tag{2.7}$$

$$\frac{dB(z)}{dz} = -jk_{21}A(z)\exp(-2j\delta z), \tag{2.8}$$

where k_{12} and k_{21} are the coupling coefficients and δ is the phase mismatch between the two modes. We will discuss, in more details, these coupled-mode equations in the following section.

2.2 Coupled-Mode Theory for Parallel Waveguides

Interaction between parallel waveguides is an important phenomenon which arises in integrated optics, fiber optics, and semiconductor laser devices. This interaction can of course be studied by solving Maxwell's equations and related boundary conditions for the normal modes of the compound waveguide structure. However, many

structures of interest cannot be easily solved using such a direct approach. Although the coupled-mode theory is approximate it has proven to be a very useful tool for studying the behavior of coupled waveguides. The accuracy of the approximate solution is fairly good as will be seen later.

Consider two parallel waveguides each supporting only one mode. When they are separated far enough, the two modes are independent of each other and their fields can be written as

$$\begin{aligned} \vec{E}_1(x,y,z) &= A\exp(-j\beta_1 z)\vec{e}_1(x,y), \\ \vec{E}_2(x,y,z) &= B\exp(-j\beta_2 z)\vec{e}_2(x,y), \end{aligned}$$

where A and B are constant amplitude coefficients which are generally complex. When brought into close proximity of each other, the two guides interact and mode coupling occurs. The presence of one waveguide in the neighborhood of the other can be regarded as a uniform deformation of the other guide. In this case the amplitude coefficients A and B are no longer constant and are not independent of each other any more. They vary along the waveguides, become functions of z, and are governed by a set of coupled-wave equations.

2.2.1 Coupled-Mode Formulations

Several approaches have been used to formulate coupled-mode equations for parallel waveguides. These approaches are based on perturbation analysis [4], reciprocity theorem [9,14], or variational principles [11,14] and all lead to couple-mode equations given in (2.7) and (2.8) or

$$\frac{da(z)}{dz} = -j\gamma_1 a(z) - jk_{12}b(z), \tag{2.9}$$

$$\frac{db(z)}{dz} = -j\gamma_2 b(z) - jk_{21}a(z). \tag{2.10}$$

The two sets of coupled-mode equations can be shown to be equivalent by substituting

$$a(z) = A(z)\exp(-j\gamma_1 z) \tag{2.11}$$

$$b(z) = B(z)\exp(-j\gamma_2 z) \tag{2.12}$$

into equations (2.9) and (2.10) and noting that the phase mismatch δ in equations (2.7) and (2.8) is

$$\delta = \frac{1}{2}(\gamma_1 - \gamma_2).$$

These formulations of coupled-mode theory differ in how the modal amplitudes ,a(z) and b(z) (or A(z) and B(z)), are defined and how the propagation constants γ_1 and γ_2 and the coupling coefficients k_{12} and k_{21} are calculated. Here we introduce a formulation derived by Yariv [4] based on the perturbation analysis mentioned in the previous section.

Conventional theory

Consider the case of two parallel single-mode slab guides with composite refractive index distribution $n_c(x)$ as illustrated in Figure 2.1. The transverse electric field of this compound waveguide structure can be approximated by the sum of the unperturbed fields; i.e., the fields of individual waveguides in isolation,

$$\vec{E}_t(x,y,z) = A(z)\,\vec{e}_{1t}^{(1)}(x)\,e^{-j\beta_1 z} + B(z)\,\vec{e}_{1t}^{(2)}(x)\,e^{-j\beta_2 z}, \tag{2.13}$$

where $\vec{e}_{1t}^{(1)}$ and $\vec{e}_{1t}^{(2)}$ are the transverse electric field associated with normal modes of waveguides 1 and 2 in isolation, respectively. The subscript '1' in the transverse normal modes indicates that they are the first mode of the guides. The perturbation polarization vector in this configuration can then be calculated as

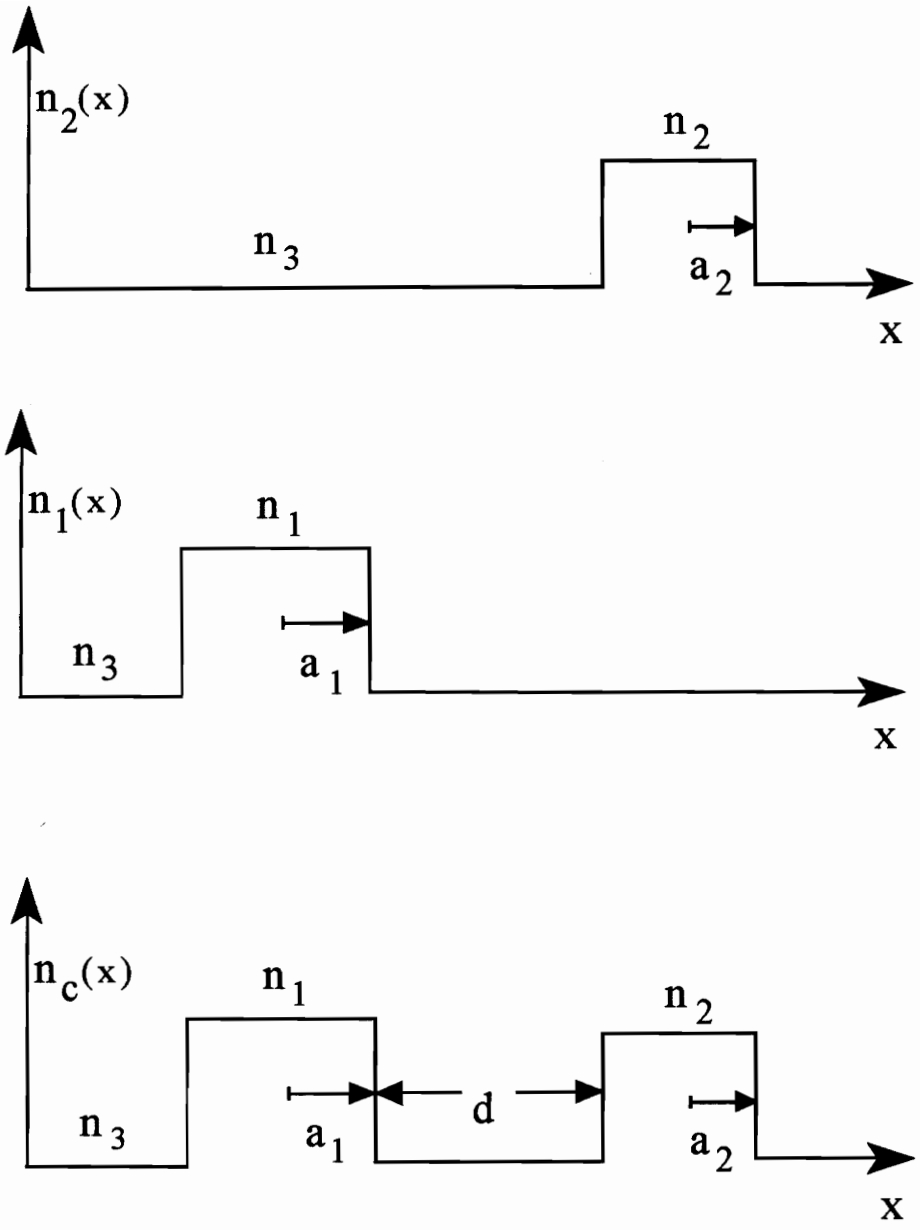

Figure 2.1: Refractive index profiles $n_1(x)$ and $n_2(x)$ for guides 1 and 2 in isolation and $n_c(x)$ for the composite structure.

$$\vec{P}_{pert} = \epsilon_0 \{ A(z)\, \vec{e}_{1t}^{(1)}(x)\, e^{-j\beta_1 z} [n_c^2(x) - n_1^2(x)] + B(z)\, \vec{e}_{1t}^{(2)}(x)\, e^{-j\beta_2 z} [n_c^2(x) - n_2^2(x)] \}, \tag{2.14}$$

where $n_1(x)$ and $n_2(x)$, as shown in Figure 2.1, are the refractive index profiles of waveguides 1 and 2 in the absence of perturbations; i.e., in isolation.

Substituting equation (2.14) into equation (2.4) and integrating over x gives

$$\frac{dA(z)}{dz} = -jk_{21}\, e^{j(\beta_1-\beta_2)z} B(z) - jk_{11} A(z) \tag{2.15}$$

$$\frac{dB(z)}{dz} = -jk_{12}\, e^{-j(\beta_1-\beta_2)z} A(z) - jk_{22} B(z), \tag{2.16}$$

where

$$k_{uv} = \frac{\omega\epsilon_0}{4} \int_{-\infty}^{\infty} [n_c^2(x) - n_v^2(x)] \vec{e}_{1t}^{(u)} \cdot \vec{e}_{1t}^{(v)} dx, \qquad u, v = 1, 2. \tag{2.17}$$

The terms k_{12} and k_{21} represent a small modification to propagation constants β_1 and β_2, respectively, caused by the presence of the second guide. If the total field is rewritten as

$$\vec{E}_t(x, y, z) = A(z)\vec{e}_{1t}^{(1)}(x)e^{-j\gamma_1 z} + B(z)\vec{e}_{1t}^{(2)}(x)e^{-j\gamma_2 z}, \tag{2.18}$$

equations (2.15) and (2.16) reduce to the coupled-mode equations (2.7) and (2.8), with phase mismatch δ defined as

$$\delta = \frac{1}{2}(\gamma_1 - \gamma_2) \tag{2.19}$$

$$\gamma_1 = \beta_1 + k_{11} \tag{2.20}$$

$$\gamma_2 = \beta_2 + k_{22}. \tag{2.21}$$

The coefficients k_{11} and k_{22} are one order of magnitude smaller than k_{12} and k_{21} and minute as compared to β_1 and β_2. Therefore, they are usually ignored and γ_1 and γ_2 are well approximated by β_1 and β_2. A coupled-mode formulation with exactly

the same definitions of coupling coefficients was also developed in [7]. Snyder [9] derived a set of coupled-mode equations with the definitions of coupling coefficients k_{12} and k_{21} being the opposite of those given by Yariv and Marcuse [4,7]. This yields different results in the nonidentical waveguide case. Before further investigating this discrepancy, we define the following integrals for the convenience of later discussions

$$C_{uv} = \frac{1}{2}\int\int_S \vec{a}_z \cdot (\vec{e}_{1t}^{(v)} \times \vec{h}_{1t}^{(u)}) dx dy, \qquad u, v = 1, 2. \tag{2.22}$$

The individual guided modes are normalized such that

$$C_{11} = C_{22} = 1.$$

The C_{12} and C_{21} coefficients are overlap integrals that describe the individual waveguide mode overlap and are a measure of the proximity of the guides. The overlap integrals are key quantities which can be used to resolve the differences between various formulations.

The coupled-mode formulations in [4,7,9] can be referred to as the *conventional theory* [13]. The common feature of these theories is that the overlap integrals are neglected in their formulations. For coupling between identical waveguides, the conventional coupled-mode theories work fine because the modes of identical guides are in fact power orthogonal and thus the overlap integrals for C_{12} and C_{21} are exactly zero. The coupling coefficient k_{12} in this case is identical to k_{21}, which is in agreement with the following relationship derived from the power conservation in lossless guides [7]

$$k_{12} = k_{21}^*. \tag{2.23}$$

However, for the case of nonidentical waveguides, several problems arise when the conventional formulations are used. First, the results are not very accurate for the

case of strong coupling between the waveguides. Secondly, the complex conjugate relationship in (2.23) does not hold any more, which means the principle of energy conservation is violated. Finally , the different results given in [4],[7] and [9] amount to exactly reversed definitions for k_{12} and k_{21}. All these problems are due to ignoring the overlap integrals;that is, assuming mode orthogonality in order to simplify the problem. Whereas, as is well known, the guided modes of the nonidentical guides are not exactly orthogonal and the overlap integrals not only do not vanish but also could be large compared to coupling coefficients in strong coupling cases. Therefore, neglecting the overlap integrals certainly causes inaccuracy.

For power to be conserved the conventional theories demand $k_{12} = k_{21}^*$. However, as is evident from the expressions in equation (2.17), k_{12} is not in general the complex conjugate of k_{21}. The reason for this inconsistency is that the relation $k_{12} = k_{21}^*$ is incorrect because it is derived by differentiating a power flow expression which does not include the overlap integrals. It should be noted that the total power is not equal to the sum of the squared moduli of the individual mode amplitude if the modes are not power orthogonal.

Improved theory

The problem of reversed definitions for k_{12} and k_{21} is an intriguing one. To resolve this seemingly contradictory situation and to reestablish the condition for power conservation, several *improved* coupled-mode formulations which take into account the overlap integrals have been proposed [11]-[15]. Hardy and Streifer [12] were the first to improve the conventional theory by including the overlap integrals. In their analysis, the radiation modes, which are usually ignored in conventional theories, are retained in the derivation and discarded only after their influence is determined. As a result,

significantly increased accuracy is achieved for the strongly-coupled nonidentical slab guides. Coupled-mode formulations in [13,14] give exactly the same definitions for the four parameters in the coupled-mode equations (2.9) and (2.10); namely modified propagation constants γ_1 and γ_2 and coupling coefficients k_{12} and k_{21}. These results differ from Hardy and Streifer's only in that formulations in [13,14] take the average values of C_{12} and C_{21} for the overlap integral. The four parameters are given as [14]

$$\gamma_1 = \beta_1 + \left[\tilde{k}_{11} + (\beta_1 - \beta_2)\bar{C}^2 - \tilde{k}_{12}\bar{C}\right]/(1-\bar{C}^2) \tag{2.24}$$

$$\gamma_2 = \beta_2 + \left[\tilde{k}_{22} + (\beta_2 - \beta_1)\bar{C}^2 - \tilde{k}_{21}\bar{C}\right]/(1-\bar{C}^2) \tag{2.25}$$

$$k_{12} = \left[\tilde{k}_{21} + (\beta_1 - \beta_2 - \tilde{k}_{22})\bar{C}\right]/(1-\bar{C}^2) \tag{2.26}$$

$$k_{21} = \left[\tilde{k}_{12} + (\beta_2 - \beta_1 - \tilde{k}_{11})\bar{C}\right]/(1-\bar{C}^2), \tag{2.27}$$

where

$$\bar{C} = \frac{(C_{12}+C_{21})}{2} \tag{2.28}$$

$$\tilde{k}_{uv} = \frac{\omega\epsilon_0}{4}\int\int_S (n_c^2 - n_v^2)\left[\vec{e}_{1t}^{(u)}\cdot\vec{e}_{1t}^{(v)} - \frac{n_u^2}{n_c^2}e_{1z}^{(u)}e_{1z}^{(v)}\right]dxdy \qquad u,v = 1,2. \tag{2.29}$$

The conservation of power is maintained by including the overlap term $\bar{C}$ and requiring that

$$k_{12} - k_{21} = \bar{C}(\gamma_1 - \gamma_2), \tag{2.30}$$

or equivalently,

$$\tilde{k}_{12} - \tilde{k}_{21} = \bar{C}(\beta_1 - \beta_2). \tag{2.31}$$

From the equations (2.30) and (2.31) we can easily see the problem of power conservation with the conventional theories. The exclusion of the overlap integral (i.e.,$\bar{C} = 0$) inevitably demands that $k_{12} = k_{21}$, no matter whether the guides are in synchronism or not, which is not true for nonidentical guides as was already indicated. Only when

the guides are close to synchronism (e.g., identical guides) or are far apart from each other (i.e., $\bar{C} \approx 0$) the relation $k_{12} = k_{21}$ is reasonably satisfied. If we apply the condition of power conservation of equation (2.31) to equations (2.24)-(2.27), we will obtain another set of four parameters as follows

$$\gamma_1 = \beta_1 + (\tilde{k}_{11} - \tilde{k}_{21}\bar{C})/(1 - \bar{C}^2) \tag{2.32}$$

$$\gamma_2 = \beta_2 + (\tilde{k}_{22} - \tilde{k}_{12}\bar{C})/(1 - \bar{C}^2) \tag{2.33}$$

$$k_{12} = (\tilde{k}_{12} - \tilde{k}_{22}\bar{C})/(1 - \bar{C}^2) \tag{2.34}$$

$$k_{21} = (\tilde{k}_{21} - \tilde{k}_{11}\bar{C})/(1 - \bar{C}^2). \tag{2.35}$$

To see the conflict about the definitions of k_{12} and k_{21}, we should compare the two sets of expressions in (2.24)-(2.27) and (2.32)-(2.35). If we neglect the overlap $\bar{C}$ in equations (2.26) and (2.27), we have

$$k_{12} = \tilde{k}_{21} \tag{2.36}$$

$$k_{21} = \tilde{k}_{12}. \tag{2.37}$$

However, if we use equations (2.34) and (2.35) instead, we have

$$k_{12} = \tilde{k}_{12} \tag{2.38}$$

$$k_{21} = \tilde{k}_{21}. \tag{2.39}$$

As shown above, the definitions of k_{12} and k_{21} are reversed if a different set of expressions is chosen. This, of course, is caused by neglecting the overlap integral. If the overlap term $\bar{C}$ is included, the two sets of definitions are equivalent since one is derived from the other after the power conservation condition is applied.

The problem of reversal of k_{12} and k_{21} is addressed very clearly by Chang [13]. He identifies two formulations for coupled-mode theory in the literature, according to how

the modal amplitudes in the coupled-mode equations are defined. In one formulation, the unknown total fields of the compound waveguide structure are assumed as linear combinations of the individual waveguide modes and the coefficients in the linear combinations are chosen as the modal amplitudes in the coupled-mode equations. The total fields are thus partitioned into components corresponding to the individual waveguide modes. The modal amplitudes in this formulation are called *partition modal amplitudes* [13]. In the other formulations, the modal amplitudes are those coefficients from the representation of the total fields as a superposition of the modes of one guide only. These modes include the guided and radiation modes and form a complete set. From a vector point of view, these modal amplitudes are the projections of the total fields onto the bases in the complete set and therefore are called the *projection modal amplitudes* [13]. The conventional formulations in [4,5,7] belong to the first category, while the formulations in [9,10] belong to the second.

The transverse component of the total electric field can take one of the following forms

$$\vec{E}_t(x,y,z) = a(z)\vec{e}_{1t}^{(1)}(x,y) + b(z)\vec{e}_{1t}^{(2)}(x,y) \tag{2.40}$$

$$= \sum \bar{a}_p(z)\vec{e}_{pt}^{(1)}(x,y) \tag{2.41}$$

$$= \sum \bar{b}_p(z)\vec{e}_{pt}^{(2)}(x,y), \tag{2.42}$$

where $\sum$ indicates summation of all guided and radiation modes. Amplitudes $a(z)$ and $b(z)$ in (2.40) are the partition modal amplitudes, while $\bar{a}_p(z)$ and $\bar{b}_p(z)$ in (2.41) and (2.42) are the projection modal amplitudes. The partition and projection modal amplitudes are different quantities but can be related as

$$\bar{a}_1(z) = a(z) + \bar{C}b(z) \tag{2.43}$$

$$\bar{b}_1(z) = b(z) + \bar{C}a(z). \tag{2.44}$$

In summary, two sets of modal amplitudes are identical when $\bar{C} = 0$, which happens only if two guides are identical. The four parameters $\gamma_1, \gamma_2, k_{12}$ and k_{21} are defined as in equations (2.24)-(2.27) if we use the partition modal amplitudes $a(z)$ and $b(z)$ as the variables in the coupled-mode equations. Changing the variables to projection modal amplitudes by substituting the relations (2.43) and (2.44) into the coupled-mode equations (2.9) and (2.10), we obtain the second set of definitions for $\gamma_1, \gamma_2, k_{12}$ and k_{21} as given in equations (2.32)-(2.35). As was already discussed, neglecting the overlap term$\bar{C}$ in different sets of definitions results in reversed definitions for k_{12} and k_{21}.

Chapter 3

Directional Coupler

One important application of coupled-mode theory is in the analysis of the directional coupler which, in its simplest form, consists of two parallel waveguides close to each other. Because of the coupling process, the optical power carried by the two guides are exchanged periodically along the direction of wave propagation z. As will be shown, the coupling process is governed by coupling coefficients k_{12}, k_{21}, and the difference between the modified propagation constants $2\delta(= \gamma_1 - \gamma_2)$. Under some proper condition, a light wave launched into one guide can be largely, or even completely, transferred to the other guide, while under a different condition the light wave can go straight through. By this behavior, directional couplers may be used as power divider, switch/modulator, or wavelength filter.

3.1 Coupled-Mode Solutions

Prior to discussing the operation of a directional coupler, it is essential to investigate the coupled-mode equations in more detail. The solutions of coupled-mode

equations in (2.7) and (2.8) are obtained as

$$a(z) = A_e\, e^{-j\beta_e z} + A_o\, e^{-j\beta_o z} \tag{3.1}$$

$$b(z) = B_e\, e^{-j\beta_e z} + B_o\, e^{-j\beta_o z}, \tag{3.2}$$

where

$$A_e = \frac{1}{2}\left(1+\frac{\delta}{s}\right) a(0) + \frac{k_{12}}{2s}\, b(0) \tag{3.3}$$

$$A_o = \frac{1}{2}\left(1-\frac{\delta}{s}\right) a(0) - \frac{k_{12}}{2s}\, b(0) \tag{3.4}$$

$$B_e = \frac{s}{2k_{12}}\left(1-\frac{\delta^2}{s^2}\right) a(0) + \frac{1}{2}\left(1-\frac{\delta}{s}\right) b(0) \tag{3.5}$$

$$B_o = \frac{-s}{2k_{12}}\left(1-\frac{\delta^2}{s^2}\right) a(0) + \frac{1}{2}\left(1+\frac{\delta}{s}\right) b(0) \tag{3.6}$$

$$\delta = \frac{\gamma_1 - \gamma_2}{2} \tag{3.7}$$

$$s = \sqrt{k_{12}k_{21} + \delta^2} \tag{3.8}$$

$$\beta_e = \frac{\gamma_1 + \gamma_2}{2} + s \tag{3.9}$$

$$\beta_o = \frac{\gamma_1 + \gamma_2}{2} - s \tag{3.10}$$

$$a(0) = a(z=0) \tag{3.11}$$

$$b(0) = b(z=0). \tag{3.12}$$

The total transverse electric field of the directional coupler can then be expressed as

$$\begin{aligned}\vec{E}_t(x,y,z) &= a(z)\,\vec{e}_{1t}^{(1)}(x,y) + b(z)\,\vec{e}_{1t}^{(2)}(x,y) \\ &= c_e\,\vec{\psi}_e(x,y)e^{-j\beta_e z} + c_o\,\vec{\psi}_o(x,y)e^{-j\beta_o z},\end{aligned} \tag{3.13}$$

where

$$c_e\,\vec{\psi}_e(x,y) = A_e\,\vec{e}_{1t}^{(1)}(x,y) + B_e\,\vec{e}_{1t}^{(2)}(x,y)$$

$$c_o\,\vec{\psi}_o(x,y) = A_o\,\vec{e}_{1t}^{(1)}(x,y) + B_o\,\vec{e}_{1t}^{(2)}(x,y),$$

and $\vec{\psi}_e(x,y)$ and $\vec{\psi}_o(x,y)$ represent normalized even and odd electric fields. From equation (3.13), we observe that the total field of the composite waveguide consists of two normal modes: $\vec{\psi}_e(x,y)$ with propagation constant β_e and $\vec{\psi}_o(x,y)$ with propagation constant β_o. The modal amplitudes are dependent on the initial excitation conditions. The modal shapes $\vec{\psi}_e$ and $\vec{\psi}_o$ are dependent not only on the characteristics of the individual guides but also on the distance between them. In general, $\vec{\psi}_o$ and $\vec{\psi}_e$ are not orthogonal. However, if the guides are identical, it follows that

$$\begin{aligned} \gamma_1 &= \gamma_2 \equiv \beta \\ \delta &= 0 \\ s &= k_{12} = k_{21} \equiv k \end{aligned}$$

and thus

$$\begin{aligned} A_e &= B_e = \frac{1}{2}\left[a(0)+b(0)\right] \\ A_o &= -B_o = \frac{1}{2}\left[a(0)-b(0)\right]. \end{aligned}$$

The total field can then be written as

$$\vec{E}_t = \frac{\sqrt{2}}{2}\left[a(0)+b(0)\right]\vec{\psi}_e e^{-j\beta_e z} + \frac{\sqrt{2}}{2}\left[a(0)-b(0)\right]\vec{\psi}_o e^{-j\beta_o z}, \tag{3.14}$$

where

$$\vec{\psi}_e = \frac{\vec{e}_{1t}^{(1)} + \vec{e}_{1t}^{(2)}}{\sqrt{2}} \tag{3.15}$$

$$\vec{\psi}_o = \frac{\vec{e}_{1t}^{(1)} - \vec{e}_{1t}^{(2)}}{\sqrt{2}} \tag{3.16}$$

$$\beta_e = \beta + k \tag{3.17}$$

$$\beta_o = \beta - k. \tag{3.18}$$

As illustrated in Figure 3.1, the modal field $\vec{\psi}_e$ is an even mode with $\beta_e = \beta + k$ and $\vec{\psi}_o$ is an odd mode with $\beta_o = \beta - k$.

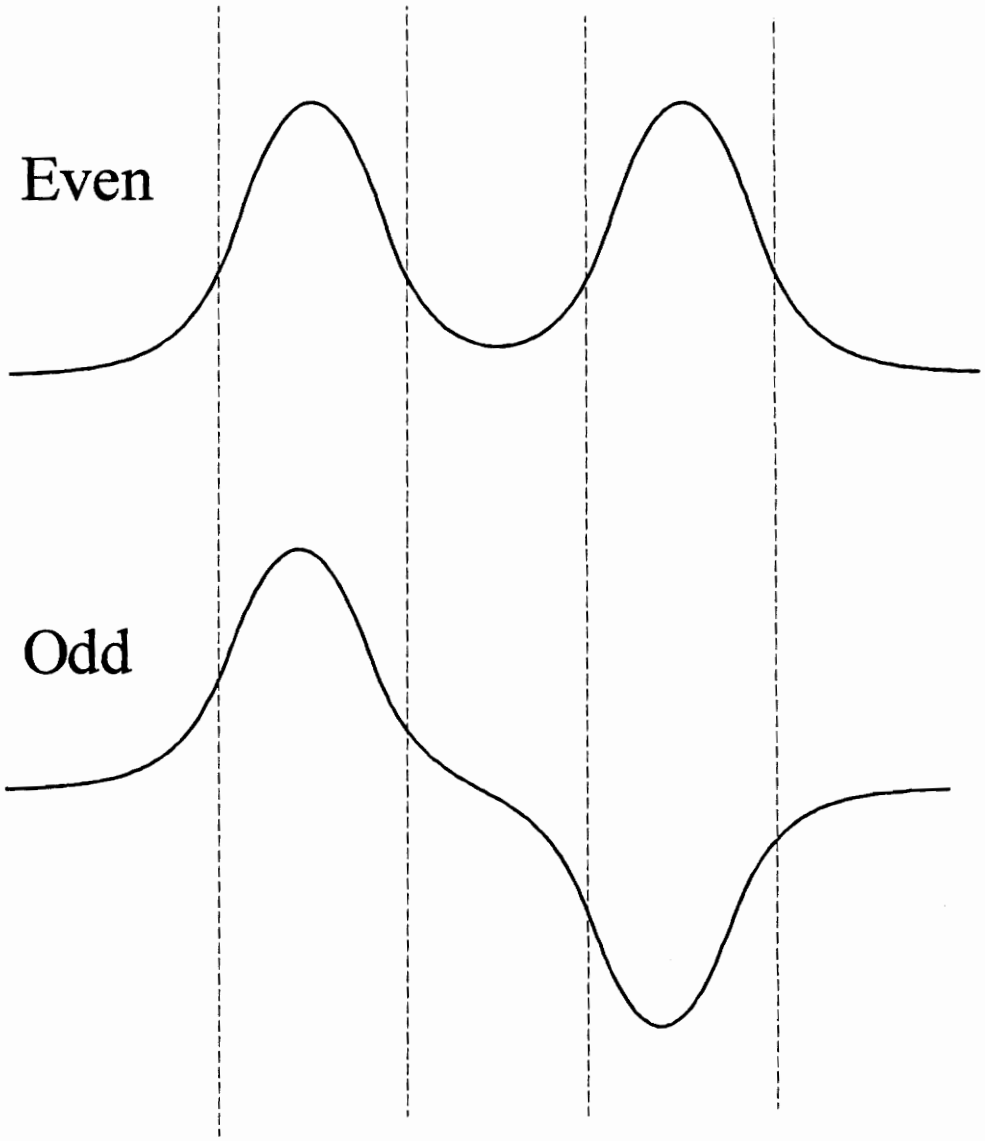

Figure 3.1: Modal shapes for the even and odd modes of a directional coupler made of identical waveguide.

It can be easily seen from Figure 3.1 or simply from

$$\vec{\psi}_e \cdot \vec{\psi}_o = \frac{1}{2}\left(|\vec{e}_{1t}^{(1)}|^2 - |\vec{e}_{1t}^{(2)}|^2 - \vec{e}_{1t}^{(1)} \cdot \vec{e}_{1t}^{(2)} + \vec{e}_{1t}^{(2)} \cdot \vec{e}_{1t}^{(1)}\right) = 0, \tag{3.19}$$

that $\vec{\psi}_e$ and $\vec{\psi}_o$ are mutually orthogonal.

Consider the case that light is launched only into waveguide 2 (i.e.,$a(0) = 0$). Equations (3.1) and (3.2) can be expressed in power forms as

$$P_1(z) = |a(z)|^2 = P_0 \frac{k_{12}^2}{s^2} \sin^2(sz) \tag{3.20}$$

$$P_2(z) = |b(z)|^2 = P_0 \left[\frac{\delta^2}{s^2} \sin^2(sz) + \cos^2(sz)\right], \tag{3.21}$$

where

$$P_0 = |b(0)|^2 = \textit{initial power}$$

The maximum power transferred to guide 1 at $z = L$ occurs when $L = \frac{\pi}{2s}$ and is obtained from

$$\left(\frac{P_1}{P_0}\right)_{max} = \frac{k_{12}^2}{k_{12}k_{21} + \delta^2}. \tag{3.22}$$

If the two guides are phase-matched (i.e., $\delta = 0$ and $k_{12} = k_{21}$), the R.H.S. of the above equation becomes 1, indicating that power is completely transferred to guide 1. When there is a phase mismatch δ, $P_1(z)/P_0$ is always smaller than 1, indicating that complete power transfer does not occur. As δ increases the amount of power transferred to guide 1 decreases. Appreciable transfer of power requires that

$$\delta < \sqrt{k_{12}k_{21}}. \tag{3.23}$$

Variations of $P_1(z)$ and $P_2(z)$ versus z for the phase-matched and non-phase-matched cases are shown in Figure 3.2. A directional coupler is a power divider and any power splitting ratio can be accomplished by proper adjustment of the coupling length, as can be seen from Figure 3.2.

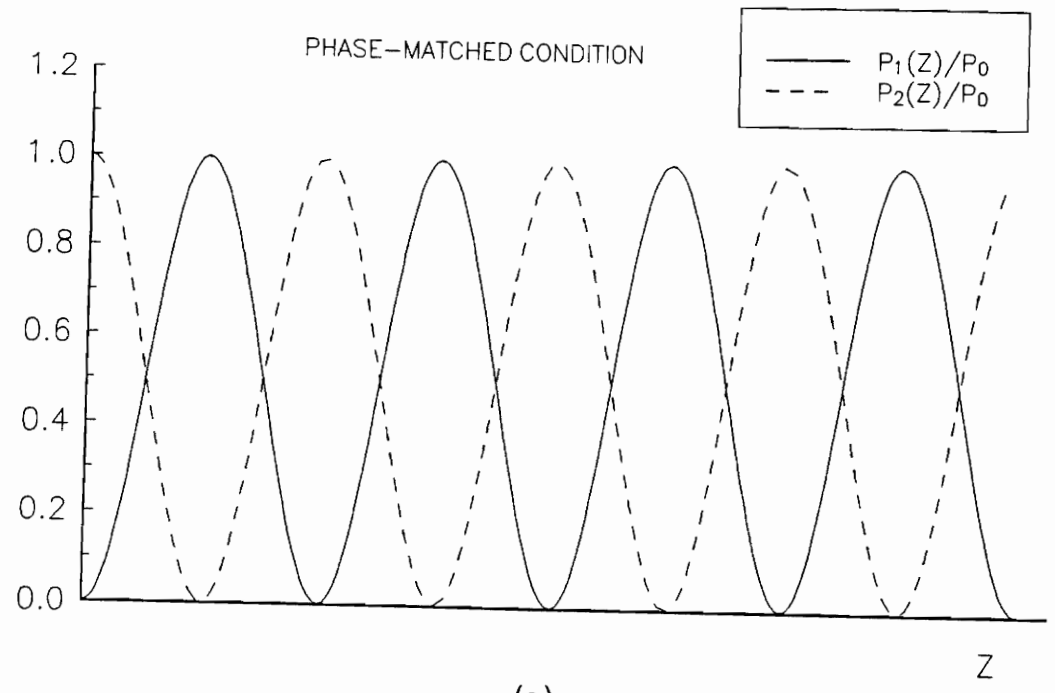

(a)

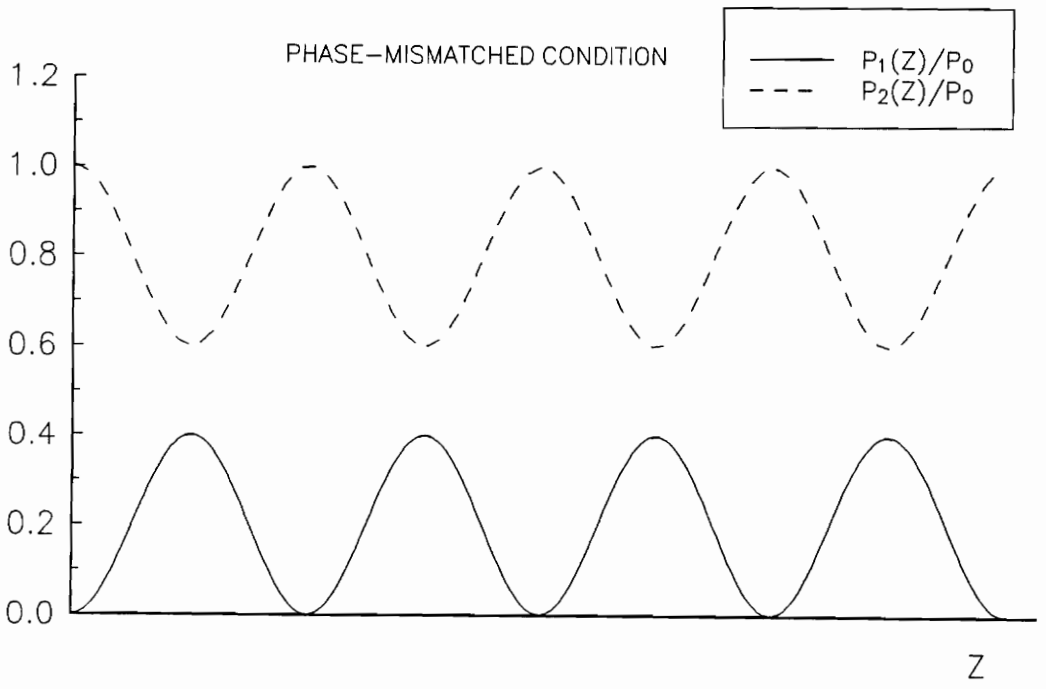

(b)

Figure 3.2: Interchange of power between the two guides as a function of propagation distance. (a) Phase-matched condition. (b) Phase-mismatched condition.

3.2 Directional Coupler as Switch/Modulator

The dependence of the transferred power on the phase mismatch can be utilized to make electrically controlled directional couplers. Integrated optics devices are usually fabricated on substrates such as $LiNbO_3$ and $GaAs$ which exhibit a strong electro-optic effect (i.e., the refractive index is changed by applying an electric field). The most common integrated-optic directional couplers are fabricated by diffusing two identical single-mode titanium (Ti) waveguides into $LiNbO_3$ substrates.

As was pointed out, light wave incident in one guide completely transfers to the other (crossover state) after a specific distance $L = \frac{\pi}{2s}$. This length is called the *transfer length*. An electric field applied through electrodes causes a differential refractive index change which eventually introduces a phase mismatch. If a proper voltage is applied such that a mismatch $\delta = \frac{\sqrt{3}\pi}{2L}$ is induced, the directional coupler is switched to the straight-through state [16]. Directional couplers operated in this regime are referred to as *uniform-*$\Delta\beta$ couplers. A major drawback of this coupler configuration is that a precise transfer length L has to be produced during device fabrication since the crossover state is not under electrical control and no voltage adjustment is available to compensate for the fabrication error. For this reason the *alternating-*$\Delta\beta$ directional coupler, which allows for electrical tuning for both states, has been proposed [17]. In this configuration, the electrodes are placed over the waveguides as the *uniform-*$\Delta\beta$ case with the difference that the polarity of the voltage and hence the phase mismatch are reversed at the midpoint of the guides. Both switching states may be obtained by employing two appropriate voltages without precise control of the transfer length. Directional coupler switches employing this mode of operation have achieved crosstalk of $-30\ dB$ or less [18].

The directional coupler modulator is a phase modulator with phase modulation proportional to the applied electric field. The phase modulation is converted to amplitude (or intensity) modulation through the coupling process. The modulation could be in a digital or an analog form. As a digital modulator, it is dc biased in the crossover state and switched to straight-through state with a modulating voltage. For analog modulation, the coupler is biased at the midpoint of a linear region and operated in the neighborhood of this linear region.

3.3 Directional Coupler as Wavelength Filter

In addition to power dividers and switches/modulators, directional couplers can be designed as wavelength filters to perform multiplexing/demultiplexing in optical communication systems. For couplers with identical guides, this application is made possible by the fact that coupling strength is wavelength-dependent. A directional coupler allowing a complete power transfer at certain wavelengths will become less effective as wavelength deviates from those wavelengths. However, the couplers made of identical waveguides do not take advantage of the phase mismatch to enhance the ability for wavelength discrimination. Therefore, most directional coupler filters are made of two nonidentical waveguides. Wavelength selectivity may be enhanced considerably by cascading several directional couplers [19].

Different waveguides exhibit different modal effective indices $\bar{n}(\lambda)$. Two dissimilar guides can be properly designed to achieve an equal effective index $\bar{n}$ at a desired passband center wavelength λ_c. At this wavelength, the guides are phase matched and thus a complete transfer of power can be achieved. As the incident wavelength shifts away from the center wavelength, the phase mismatch increases and consequently

the transferred power decreases. For wavelengths sufficiently far from λ_c, nearly no transfer of power occurs. Hence, directional coupler filters made of nonidentical guides display a passband response centered at λ_c as illustrated in Figure 3.3.

The fractional bandwidth of a directional coupler filter is given by [20]

$$\frac{\Delta\lambda}{\lambda} = \frac{1}{L}\left[\frac{d}{d\lambda}(\bar{n}_2 - \bar{n}_1)\right]^{-1}_{\lambda=\lambda_c}, \tag{3.24}$$

where $\bar{n}_1$ and $\bar{n}_2$ are effective indices of guides 1 and 2, respectively. As seen from the above equation, a narrower spectral width is obtained with a greater coupling length and a larger intersection angle of the two modal dispersion curves.

The directional coupler filter can be readily electrically tuned by the use of uniform-$\Delta\beta$ or alternating-$\Delta\beta$ configuration described earlier. The applied electric field moves the phase-matched wavelength to a new point and results in a new center wavelength for the filter.

Directional coupler filters have been fabricated with both $Ti\text{-}LiNbO_3$ and $InGaAsP/InP$ waveguides. However, electrical tuning has been demonstrated only for the $Ti\text{-}LiNbO_3$ filter. An $InGaAsP/InP$ filter is a *vertical* directional coupler in the sense that two guiding regions are formed by two epitaxially grown planar waveguides. The vertical wavelength selective coupling is essential to the operation of $InGaAsP/InP$ semiconductor lasers which contain an active gain region and a low-loss passive waveguide reflector region [21].

The presence of sidelobes limits the number of channels when filters are used to perform wavelength demultiplexing. Sidelobe reduction can be achieved by weighting the coupling coefficients along the interaction length. One simple way of implementing this is to taper the space between the two guides [22]. A fiber directional coupler filter with tapered interguide spacing has been reported to have a FWHM (full width at a

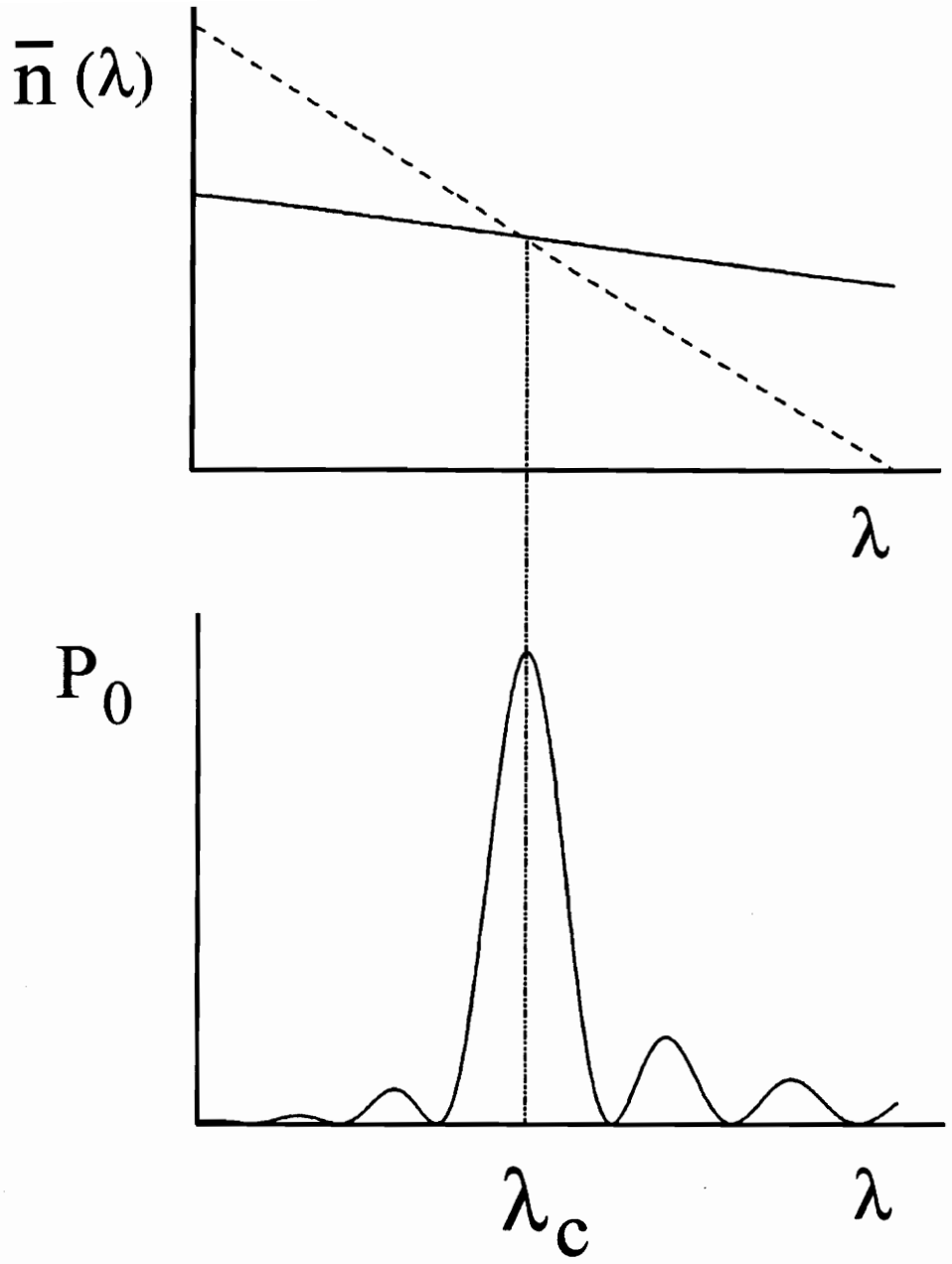

Figure 3.3: Directional coupler filter centered at λ_c. Maximum transfer of power occurs when phases of the two guides are matched at λ_c.

half maximum or 3 dB bandwidth) bandwidth of 22.5 nm and a maximum sidelobe of -11 dB [23].

Chapter 4

Optical Resonator - Fabry-Perot Etalon

An optical resonator may be regarded as an optical transmission medium incorporating a feedback mechanism. Light at certain wavelengths can travel back and forth repeatedly without destructive interference and thus energy is confined and stored within the resonator. The archetype of optical resonators, known as *Fabry-Perot (F-P) etalon*, consists of two parallel, highly reflective, planar mirrors separated by a distance L. The F-P etalon has two major applications: first, it forms a cavity resonator for lasers. Secondly, its wavelength selectivity property makes it useful as a narrowband transmission filter or a spectrum analyzer.

4.1 Fabry-Perot Etalon - Laser Cavity Resonator

A laser cavity contains a medium that amplifies light. A resonant mode is a wave that reproduces itself after a complete round trip. This results in two conditions, phase and amplitude conditions, for steady-state oscillations [24]. The phase condition gives

$$2\beta L = 2m\pi \qquad m = 1, 2, 3 \ldots, \tag{4.1}$$

which determines the resonant frequencies of the F-P resonator. The amplitude condition requires that the gain of the medium g be equal to the total loss α_t; that is,

$$g = \alpha_t = \alpha_s + \frac{1}{L}\ln(\frac{1}{r_1 r_2}), \tag{4.2}$$

where r_1 and r_2 are reflection coefficients of the mirrors and α_s represents the attenuation coefficient due to scattering and absorption. The last term in equation (4.2) represents the transmission losses of the mirrors.

The net field in an optical resonator is the summation of an infinite number of waves whose complex amplitudes form a geometrical progression. The spectral response of a F-P resonator is then calculated as [25]

$$I = \frac{I_{max}}{1 + (2F/\pi)^2 \sin^2(\pi f/\Delta_f)}, \tag{4.3}$$

where

$$\begin{aligned}
I_{max} &= \frac{I_0}{(1 - r_1 r_2)^2} \\
F &= \frac{\pi\sqrt{r_1 r_2}}{1 - r_1 r_2} \\
\Delta_f &= \frac{\pi f}{\beta L} = \frac{c}{2\bar{n}L} \\
I_0 &= \textit{intensity of the initial wave} \\
f &= \textit{frequency of light} \\
\bar{n} &= \textit{effective index of cavity medium} \\
c &= \textit{speed of light in free space.}
\end{aligned}$$

Equation (4.3) indicates that the spectral response reaches maximum when

$$f = m\Delta_f \qquad m = 1, 2, 3 \ldots .$$

This condition is equivalent to the resonant condition in equation (4.1) and we can conclude that the peak response occurs at resonant frequencies.

4.2 F-P Resonator as Wavelength Filter

When a F-P etalon is used as a wavelength filter, an optical wave incident on one end is transmitted through and exits from the other end. The intensity transmittance is given by [25]

$$\mathcal{T}(f) = \frac{I_t}{I_i} = \frac{T_{max}}{1 + (2F/\pi)^2 \sin^2(\pi f/\Delta_f)}, \tag{4.4}$$

where

$$\begin{aligned} T_{max} &= \frac{(t_1 t_2)^2}{(1 - r_1 r_2)^2} \\ t_1, t_2 &= \textit{transmission coefficients of mirrors} \\ I_i &= \textit{incident intensity} \\ I_t &= \textit{transmitted intensity.} \end{aligned}$$

The transmittance $\mathcal{T}(f)$ has the same dependence on frequency f as that of the spectral response of a resonator cavity. Therefore, transmittance is maximum when frequency of the incident wave coincides with one of the resonant frequencies.

The parameter F in equations (4.3) and (4.4) is known as the *finesse* and defined as the ratio of the separation between peaks (i.e.,Δ_f) to the FWHM. It is a measure of resolution of a F-P filter. The resolution increases with F. For resonators with perfect mirrors, F is infinity and the resolution power is unlimited. The tuning range of the F-P filter is limited to the spacing of the transmittance peaks Δ_f which is called the *free spectral range* (FSR). FSR can be also expressed in terms of wavelength as

$$FSR = \frac{\lambda^2}{2\bar{n}L} . \tag{4.5}$$

A typical transmittance function $\mathcal{T}(\lambda)$ of a single cavity F-P etalon is shown in Figure 4.1.

The filter is tuned by adjusting the distance L between mirrors. F-P filters with ultrahigh finesse (F of order of 500 at $\lambda = 1.5\mu m$) have been fabricated successfully [26]. The FWHM bandwidth of these filters was reported to be below 1 MHz.

4.3 Multiple Cavity Fabry-Perot Filters

The F-P filter described in the previous section is a two-mirror single-cavity interferometer. The performance of F-P filters can be improved tremendously by employing multiple cavity structures, which may be realized by adding one or more mirrors to a two-mirror F-P etalon (multimirror structure) or placing two or more single-cavity F-P filter in tandem (multicavity structure). A high-finesse filter can be made of single cavity filters with moderate finesses. In this section, only the three-mirror filter and the dual-cavity filter with two separate cavities is briefly discussed. Extension to multimirror and multicavity cases is quite straightforward.

4.3.1 Three-Mirror F-P Filter

The power transmittance spectrum of a three-mirror F-P filter is [28,27]

$$\mathcal{T}(f) = \frac{(t_1 t_2 t_0)^2}{|1 - r_1 r_0 \exp(-j2\phi_1) + r_2 r_0 \exp(-j2\phi_2) - r_1 r_2 \exp[-j2(\phi_1 + \phi_2)]|^2} \tag{4.6}$$

where

$$r_1, r_2, t_1, t_2 \;=\; \textit{end mirror reflection and transmission coefficients (from inside to outside of cavity)}$$

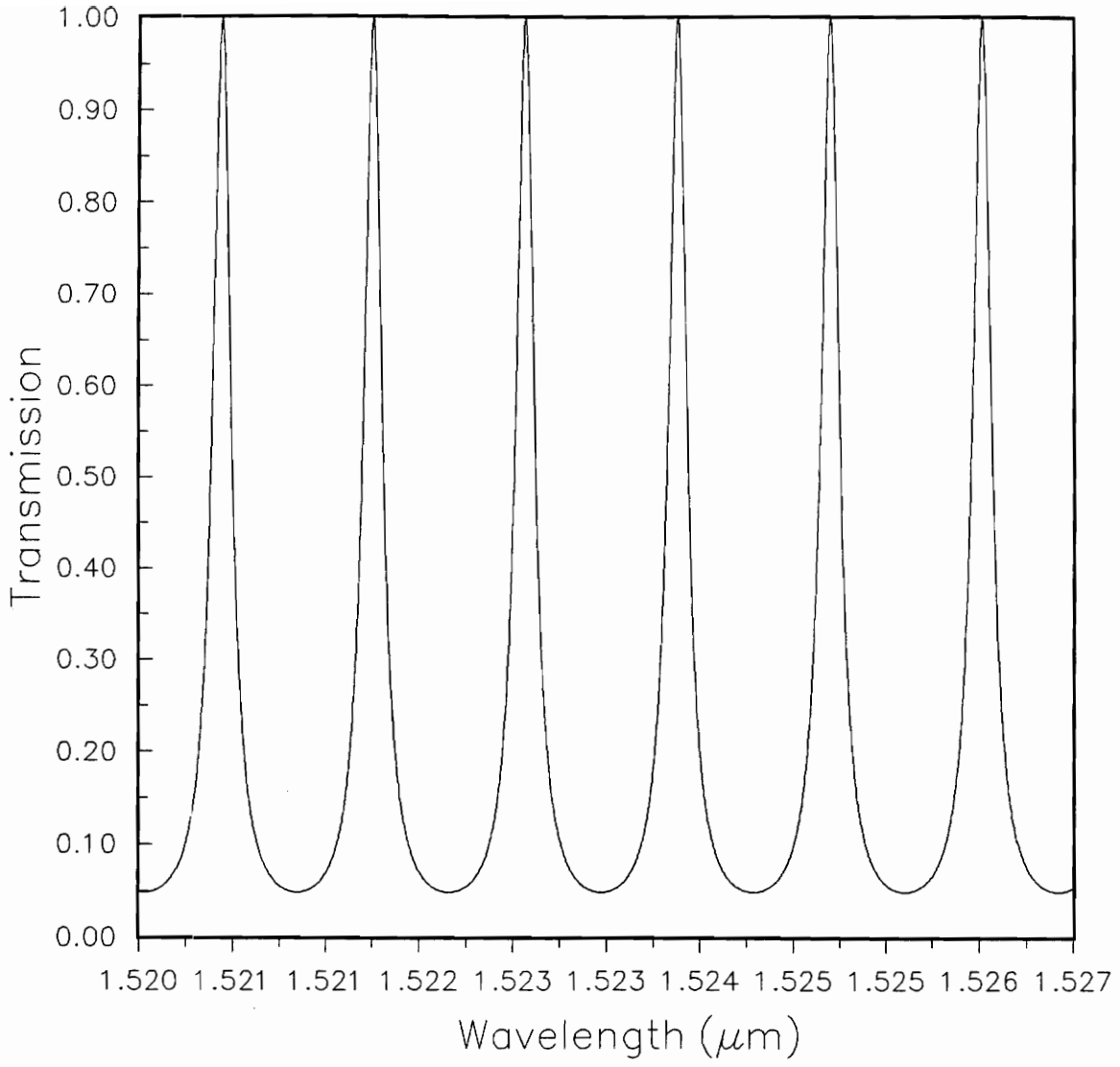

Figure 4.1: Transmittance v.s. λ for a Fabry-Perot etalon.

$$
\begin{aligned}
r_0, t_0 &= \textit{central mirror reflection and transmission coefficients} \\
&\quad (\textit{from cavity 1 to cavity 2}) \\
\phi_i &= \frac{\pi f}{\Delta_f^i} \qquad\qquad i = 1, 2 \\
\Delta_f^i &= FSR_i = \textit{free spectral range of the } i^{th} \textit{ cavity.}
\end{aligned}
$$

It should be noted that r_1 here is the negative of r_1 in [28] because the directions of reflection are opposite. It can be shown that equation (4.6) has maximum transmittance (i.e., unity) when

$$\exp(-j2\phi_1) = \exp(-j2\phi_2) = 1, \tag{4.7}$$

and

$$r_0 = \frac{r_1 - r_2}{1 - r_1 r_2}. \tag{4.8}$$

Equation (4.7) implies that both cavities are at resonance. For r_0 as given in equation (4.8), only lightwaves with frequencies at which both cavities simultaneously resonate can have 100% transmission. So it is evident that this filter has much higher wavelength selectivity than the conventional two- mirror F-P filter. The equivalent FSR of this three-mirror filter is given by [27]

$$FSR_{eq} = \frac{FSR_1 \cdot FSR_2}{|FSR_2 - FSR_1|}. \tag{4.9}$$

If FSR_1 and FSR_2 are only slightly different, it is evident from (4.9) that FSR_{eq} can be many times larger than the individual FSRs. The tuning range is thus significantly improved. If the lengths of cavities 1 and 2, denoted as L_1 and L_2, are chosen as $L_1 = 160\ \mu m$ and $L_2 = 140\ \mu m$, from (4.5), $FSR_2 = 8/7\ FSR_1$. The transmittance spectrum of this three-mirror F-P filter is shown in Figure 4.2. Figure 4.3 shows transmittance of another three-mirror F-P filter with $L_1 = 155\ \mu m$ and $L_2 = 145\ \mu m$.

As seen from Figures 4.2 and 4.3, each filter has a multiple-fold improvement in tuning range. As the difference between FSR_1 and FSR_2 decreases, FSR of the filter increases but so do the sidelobes.

To see how the FWHM bandwidth is improved, for simplicity, we assume that FWHM bandwidth is approximately the same for both cavities and $r_1 = r_2$. If FWHM of each cavity is W, the FWHM bandwidth of three-mirror filter is obtained as

$$FWHM_{eq} = \frac{W}{\sqrt{2}}.$$

Therefore, utilizing the multimirror filter structure not only increases the tuning range significantly but also reduces the FWHM bandwidth and consequently results in a much higher finesse.

4.3.2 Dual-Cavity F-P Filter

We consider two cases of dual-cavity structures: (a) two single cavity F-P filters separated by an optical isolator, and (b) the separation of two cavities is larger than the coherence length L_c of the light sources employed.

The isolator is used to suppress unwanted multiple reflections within the intercavity region. Again we assume $FSRs$ are slightly different and FWHM bandwidths are approximately equal. If $\mathcal{T}_1(f)$ and $\mathcal{T}_2(f)$ are the transmittance functions of the two filters, then the combined transmittance of the dual-cavity structure is simply [27]

$$\mathcal{T}(f) = \mathcal{T}_1(f)\mathcal{T}_2(f). \tag{4.10}$$

$\mathcal{T}(f)$ in (4.10) is maximized when both $\mathcal{T}_1(f)$ and $\mathcal{T}_2(f)$ assume their maximum values. As in the case of three-mirror filter, only light with frequencies simultaneously

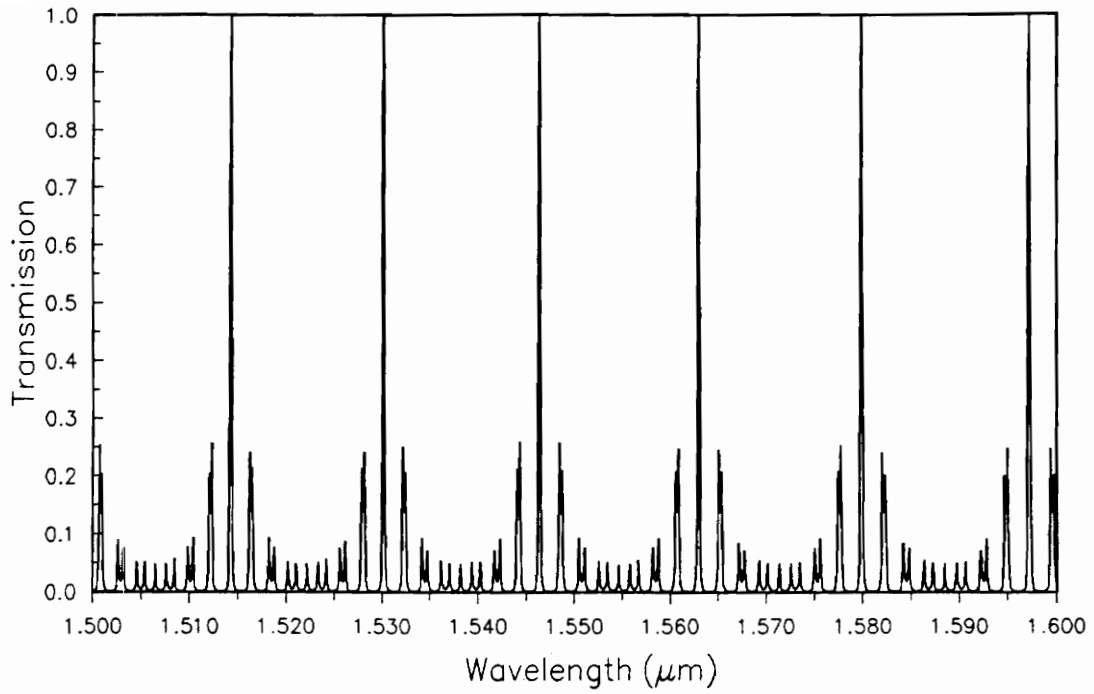

Figure 4.2: Transmittance spectrum of a three-mirror F-P filter with $FSR_2 = 8/7\ FSR_1$.

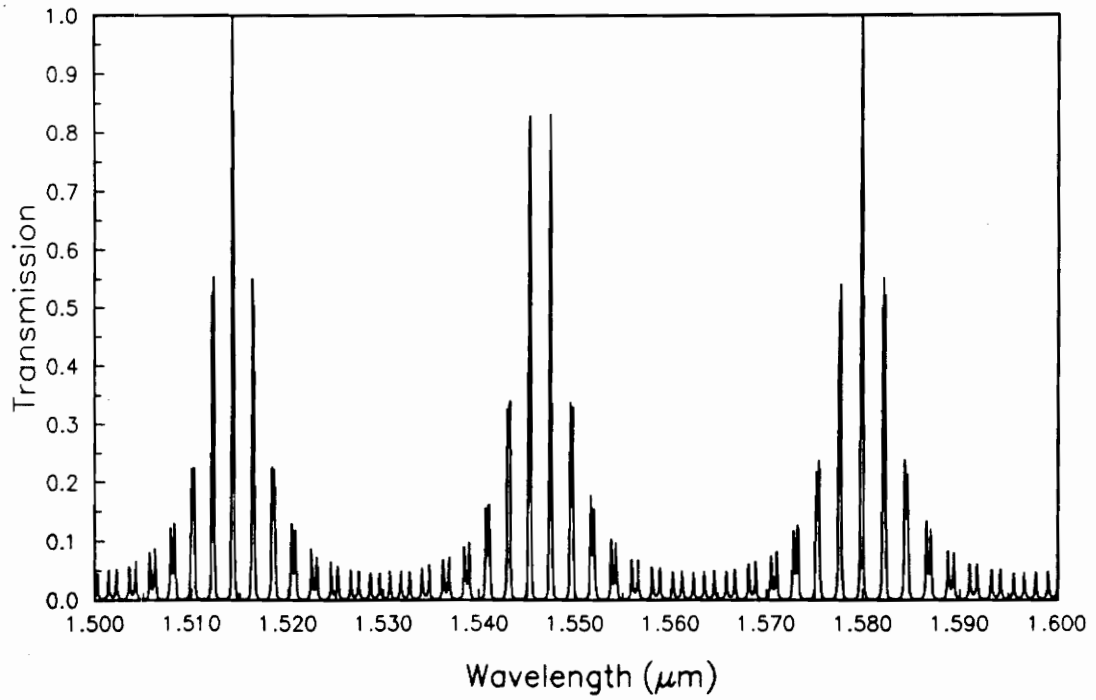

Figure 4.3: Tranmittance spectrum of a three-mirror F-P filter with $FSR_2 = 31/29\ FSR_1$.

matching the resonant frequencies of each single cavity filter has the maximum transmittance. The equivalent FSR of this filter structure is given by equation (4.9), and the FWHM bandwidth is

$$FWHM_{eq} = (\sqrt{2} - 1)^{1/2} W. \tag{4.11}$$

If the two filters are separated with a distance greater than L_c, multiple reflections within the intercavity region are added incoherently and thus no resonance in the interfilter cavity. The average transmittance of this incoherent cascade is given by [27]

$$\langle \mathcal{T}(f) \rangle = \frac{\mathcal{T}_1(f)\mathcal{T}_2(f)}{\mathcal{T}_1(f) + \mathcal{T}_2(f) - \mathcal{T}_1(f)\mathcal{T}_2(f)} . \tag{4.12}$$

It can be easily shown that maximum transmittance occurs at frequencies which maximize $\mathcal{T}_1(f)$ and $\mathcal{T}_2(f)$ at the same time. FSR is again given by (4.9) and the FWHM bandwidth is $W/\sqrt{2}$.

Both multimirror and multicavity structures improve significantly the filtering efficacy of the F-P interferometers by increasing the tuning range and decreasing the FWHM bandwidth. However, the spectrum of the multimirror structure is more square-like passband and is preferred over the multicavity structure.

Chapter 5

Coupled-Waveguide Fabry-Perot Resonator

In the previous chapters, we reviewed the coupled-mode theory and its application to the analysis of parallel waveguide structures such as directional couplers. Here, we propose a coupled-waveguide Fabry-Perot structure made of two parallel waveguides, as shown in Figure 5.1. Each guide, in isolation, can be regarded as a single cavity Fabry-Perot etalon. This configuration differs from the parallel waveguide structures described in previous chapters only in that it has reflecting mirrors at all four ends. The proposed structure can be utilized as a tuned resonator as well as a narrowband wavelength filter. Two mechanisms contribute to the operation of the structure: (1) interference of counter propagating waves resulting from reflection by the end mirrors, (2) coupling of waves between the parallel guides. Therefore, the device would exhibit the attributes of both Fabry-Perot resonator and directional coupler. The coupled-mode analysis for parallel waveguides introduced earlier is employed to explore the behavior and characteristics of this new device as a resonator and as a filter. First, we consider the simpler case of two identical guides. The more complex nonidentical

waveguides case then follows.

5.1 Structure with Identical Guides

5.1.1 Cavity Resonator

The analysis of the coupled-cavity resonator of Figure 5.2 can be facilitated by dividing the total field of the compound structure into four components: two forward traveling and two backward traveling waves. The modal amplitudes of the four waves are denoted as $A_1(z), A_2(z)$ for the forward propagating waves and $B_1(z'), B_2(z')$ for the backward propagating waves as illustrated in Figure 5.2. The co-directional coupling takes place between two forward and two backward traveling waves. Consequently, two sets of coupled-wave equations are required. These equations are expressed as

$$\frac{dA_1(z)}{dz} = -jk_{12}A_2(z)\exp(2j\delta z) \tag{5.1}$$

$$\frac{dA_2(z)}{dz} = -jk_{21}A_1(z)\exp(-2j\delta z), \tag{5.2}$$

$$\frac{dB_1(z')}{dz'} = -jk_{12}B_2(z')\exp(2j\delta z') \tag{5.3}$$

$$\frac{dB_2(z')}{dz'} = -jk_{21}B_1(z')\exp(-2j\delta z'). \tag{5.4}$$

In the case of identical guides, $\delta = 0, k_{12} = k_{21} \equiv k$ and $\gamma_1 = \gamma_2 = \beta$, then the modal amplitudes A_1 and A_2 evaluated at $z = L$ and B_1 and B_2 evaluated at $z' = L$ are easily obtained as

$$A_1(L) = A_1(0)\cos(kL) - jA_2(0)\sin(kL) \tag{5.5}$$

$$A_2(L) = -jA_1(0)\sin(kL) + A_2(0)\cos(kL), \tag{5.6}$$

and

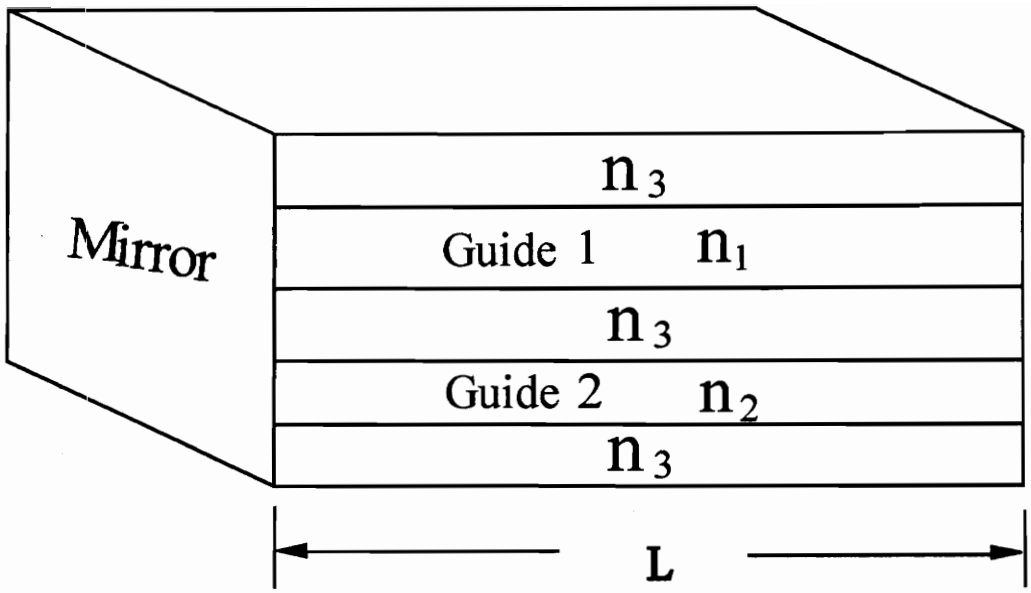

(a)

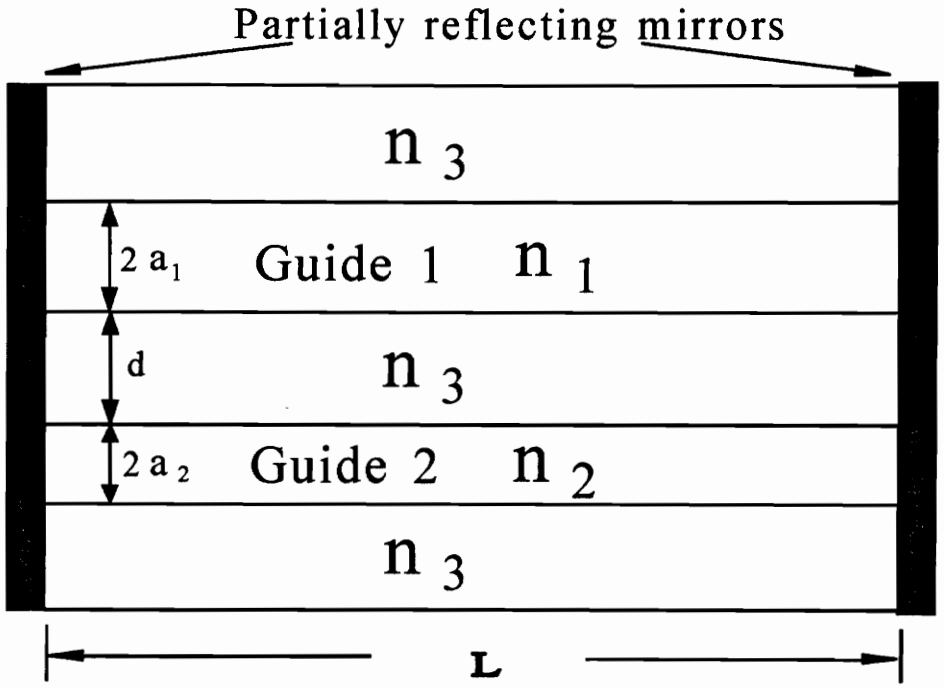

(b)

Figure 5.1: Schematic view for the proposed coupled-waveguide Fabry-Perot structure. (a) Perspective view. (b) Side view.

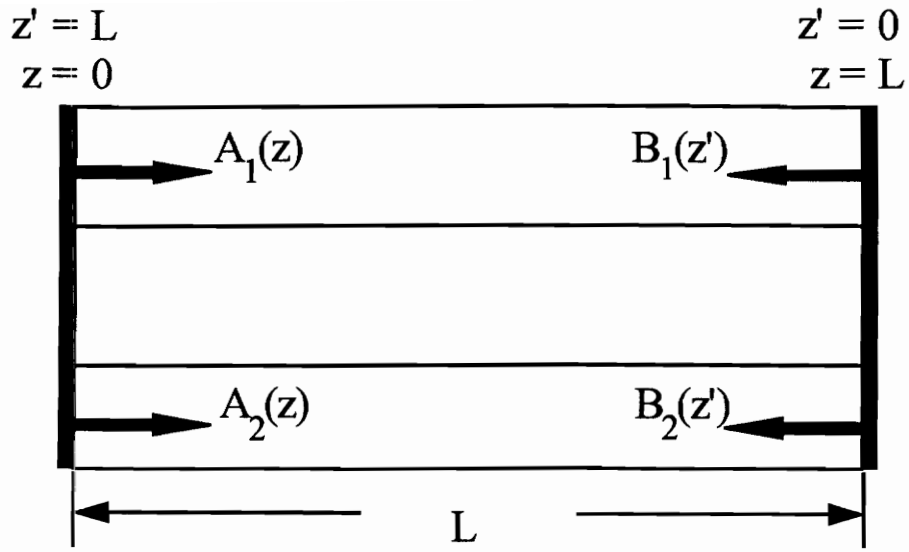

Figure 5.2: Field components in coupled-waveguide F-P resonator. Total field is divided into two forward and two backward traveling waves.

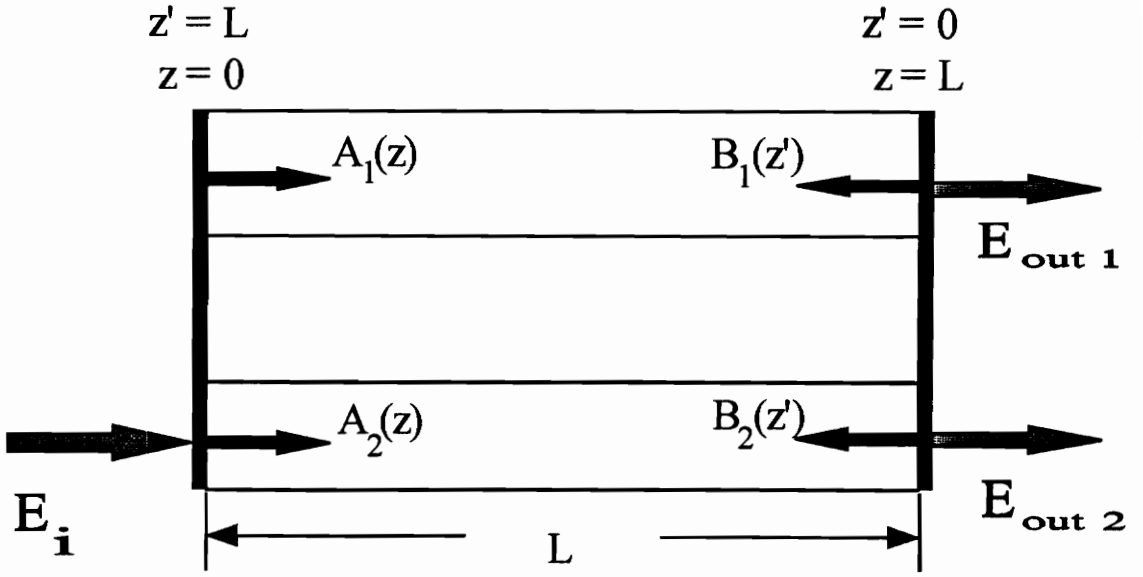

Figure 5.3: Field components in coupled-waveguide F-P resonator. The optical power is launched into guide 2.

$$B_1(L) = B_1(0)\cos(kL) - jB_2(0)\sin(kL) \tag{5.7}$$

$$B_2(L) = -jB_1(0)\sin(kL) + B_2(0)\cos(kL). \tag{5.8}$$

The forward and backward traveling waves are connected to each other at the end points, $z = 0$ $(z' = L)$ and $z = L$ $(z' = 0)$, through the following relations. These relations, in fact, constitute the boundary conditions of the problem.

$$A_1(0) = B_1(L)e^{-j\beta L}\, r_1 \tag{5.9}$$

$$A_2(0) = B_2(L)e^{-j\beta L}\, r_1 \tag{5.10}$$

$$B_1(0) = A_1(L)e^{-j\beta L}\, r_2 \tag{5.11}$$

$$B_2(0) = A_2(L)e^{-j\beta L}\, r_2, \tag{5.12}$$

where $r_{1,2}$ are the reflection coefficients of mirrors. To facilitate the calculation of resonant wavelengths, we assume that the end mirrors are perfect and the waveguides are lossless; that is, $r_{1,2} = -1$ and β is real. The case of partially reflecting end facets and lossy waveguides is considered later. Eight equations (5.5)-(5.12) which relate eight quantities $A_1(0)$, $A_2(0)$, $A_1(L)$, $A_2(L)$, $B_1(0)$, $B_2(0)$, $B_1(L)$ and $A_2(L)$ can be reduced to the following two equations

$$\frac{A_1(0)}{A_2(0)} = \frac{j\sin(2kL)}{\cos(2kL) - \exp(j2\beta L)} \tag{5.13}$$

$$\frac{A_1(0)}{A_2(0)} = \frac{\cos(2kL) - \exp(j2\beta L)}{j\sin(2kL)}. \tag{5.14}$$

To have nontrivial solutions, the right hand sides (R.H.S.) of the above two equations must be equal. That is,

$$\frac{A_1(0)}{A_2(0)} = \frac{j\sin(2kL)}{\cos(2kL) - \exp(j2\beta L)} = \frac{\cos(2kL) - \exp(j2\beta L)}{j\sin(2kL)}. \tag{5.15}$$

It is easily seen that (5.15) can be resolved into two equations given below,

$$j\sin(2kL) = \cos(2kL) - \exp(j2\beta L) \tag{5.16}$$

$$j\sin(2kL) = -\cos(2kL) + \exp(j2\beta L). \tag{5.17}$$

Solving equations (5.16) and (5.17) yields

$$(\beta + k)L = m\pi, \qquad m = 1, 2, 3\ldots \tag{5.18}$$

$$(\beta - k)L = n\pi, \qquad n = 1, 2, 3\ldots. \tag{5.19}$$

The solution in (5.18) corresponds to the case when $A_1(0)/A_2(0) = 1$ and is associated with an even mode, while the solution in (5.19) corresponds to the case when $A_1(0)/A_2(0) = -1$ and is associated with an odd mode. As described in Chapter 3, the identical parallel-waveguide structure has two fundamental modes: an even mode with propagation constant $\beta + k$ and an odd mode with propagation constant $\beta - k$. Equations (5.18) and (5.19) are clearly the phase resonance conditions for the even and odd modes in the coupled-waveguide F-P cavity. Main resonances occur when both conditions are satisfied simultaneously in which case (5.18) and (5.19) can be rewritten as

$$2\beta L = p\pi \tag{5.20}$$

$$2kL = q\pi, \tag{5.21}$$

where both p and q have to be even or odd integers. This is really a much stricter condition than that for a single cavity F-P resonator given in (4.1).

The preceding analysis is based on the assumption that mirrors are perfect and β is real. We now take into account both the medium gain and mirror losses and show that the same results as for the lossless case are obtained.

When the medium has a net distributed gain of α (Np/m), the propagation constant is complex and takes the form

$$\beta = \beta_r - j\alpha/2, \tag{5.22}$$

where β_r , the real part of propagation constant, is the phase constant. For complex β, the condition of equation (5.15) is expressed as

$$\frac{j\sin(2kL)}{\cos(2kL) - \frac{1}{r_1 r_2} e^{-\alpha L} e^{j2\beta_r L}} = \frac{\cos(2kL) - \frac{1}{r_1 r_2} e^{-\alpha L} e^{j2\beta_r L}}{j\sin(2kL)}. \tag{5.23}$$

In a laser cavity with mirror reflection coefficients r_1 and r_2, the amplitude condition (4.2) implies that

$$\alpha = g - \alpha_s \tag{5.24}$$

$$= \frac{1}{L}\ln(\frac{1}{r_1 r_2}), \tag{5.25}$$

or equivalently,

$$\frac{1}{r_1 r_2} e^{-\alpha L} = 1. \tag{5.26}$$

Substituting (5.26) into (5.23), we have the same result as that in equation (5.15).

5.1.2 Wavelength Filter

The proposed coupled-waveguide Fabry-Perot structure can also be used as a wavelength filter. As illustrated in Figure 5.3, power is launched into one guide and can emit from the opposite end of either guide. Similar to directional couplers, light at certain wavelengths can be coupled significantly into the other guide and at some other wavelengths goes straight through. In this section, we will derive the transmission characteristics of the parallel identical coupled-waveguide F-P filter.

The boundary conditions for the coupled-waveguide resonator F-P filter are slightly different from those for a cavity resonator. They can be written as

$$A_1(0) = B_1(L)e^{-j\beta L}\, r_1 \tag{5.27}$$

$$A_2(0) = B_2(L)e^{-j\beta L}\, r_1 + (1-r_1)E_i \tag{5.28}$$

$$B_1(0) = A_1(L)e^{-j\beta L}\, r_2 \tag{5.29}$$

$$B_2(0) = A_2(L)e^{-j\beta L}\, r_2, \tag{5.30}$$

where E_i is the complex amplitude of the input field. Solving equations (5.5)-(5.8) and (5.27)-(5.30), we obtain

$$A_1(L) = \left[\frac{(1-r_1)(r_1r_2 + e^{j2\beta L})\sin(kL)}{2r_1r_2\cos(2kL) - r_1^2r_2^2e^{-j2\beta L} - e^{j2\beta L}}\right] E_i \tag{5.31}$$

$$A_2(L) = \left[\frac{(1-r_1)(r_1r_2 - e^{j2\beta L})\cos(kL)}{2r_1r_2\cos(2kL) - r_1^2r_2^2e^{-j2\beta L} - e^{j2\beta L}}\right] E_i. \tag{5.32}$$

The amplitudes of the output light from the guides are expressed as

$$E_{out1} = A_1(L)e^{-j\beta L}(1+r_2) \tag{5.33}$$

$$E_{out2} = A_2(L)e^{-j\beta L}(1+r_2). \tag{5.34}$$

Substituting equations (5.31) and (5.32) into (5.33) and (5.34), the power transmittance of the guides are given by

$$\begin{aligned}\mathcal{T}_1(f) &= \left|\frac{E_{out1}}{E_i}\right|^2 \\ &= \frac{(1+r_2)^2(1-r_1)^2}{4}\left|\frac{e^{-j(\beta+k)L}}{1-r_1r_2e^{-j2(\beta+k)L}} - \frac{e^{-j(\beta-k)L}}{1-r_1r_2e^{-j2(\beta-k)L}}\right|^2\end{aligned} \tag{5.35}$$

$$\begin{aligned}\mathcal{T}_2(f) &= \left|\frac{E_{out2}}{E_i}\right|^2 \\ &= \frac{(1+r_2)^2(1-r_1)^2}{4}\left|\frac{e^{-j(\beta+k)L}}{1-r_1r_2e^{-j2(\beta+k)L}} + \frac{e^{-j(\beta-k)L}}{1-r_1r_2e^{-j2(\beta-k)L}}\right|^2.\end{aligned} \tag{5.36}$$

Transmittance functions $\mathcal{T}_1$ and $\mathcal{T}_2$ depend on frequency since β and the coupling coefficient k are dependent upon frequency. As a check on the correctness of the above two equations, we let $k = 0$ in (5.35) and (5.36), which means that the waveguides are separated far from each other. Doing so, $\mathcal{T}_1$ in (5.35) vanishes and $\mathcal{T}_2$ in (5.36) is reduced to the transmittance function of a single F-P cavity given by (4.4). This is true since light is launched into guide 2 and no optical power can be coupled to guide 1 if the two guides are far away apart from each other.

The first and second terms inside $|\cdot|$ of the R.H.S. of (5.35) and (5.36) represent the net field amplitudes of the even and odd modes, respectively. As shown in the above two equations, the output field amplitudes of guides 1 and 2 are the difference and the sum of the amplitudes of even and odd modes. This is expected since even and odd modes are the sum and difference of the modes of individual guides and vice versa. As discussed in Chapter 4, we expect maximum transmission to occur when the incident wave is a resonant mode. Consider the case of $r_1 = r_2$. If resonance conditions (5.18) and (5.19) are satisfied and m and n are both even or both odd, $\mathcal{T}_2(f)$ is unity, indicating 100% transmittance and $\mathcal{T}_1(f)$ is zero. But if either m or n is even and the other is odd, then $\mathcal{T}_1(f)$ is one and $\mathcal{T}_2(f)$ is zero.

5.1.3 Coupling Coefficient, k

Before the resonator cavity spectral response and the filter transmittance can be determined, it is necessary that we obtain an expression for coupling coefficient k. Without loss of generality, we assume a transverse-electric (TE) polarization for guided modes throughout the analysis hereafter. Since the first TE mode of individual guides, designated as TE_0 mode, is an even mode, referring to Figure 5.4 the transverse electric field distribution of each guide is expressed as

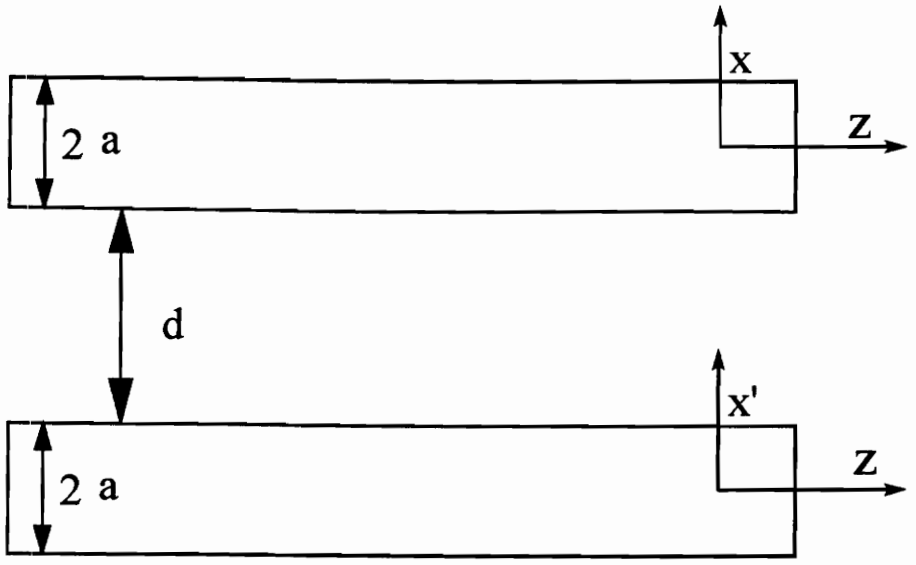

(a)

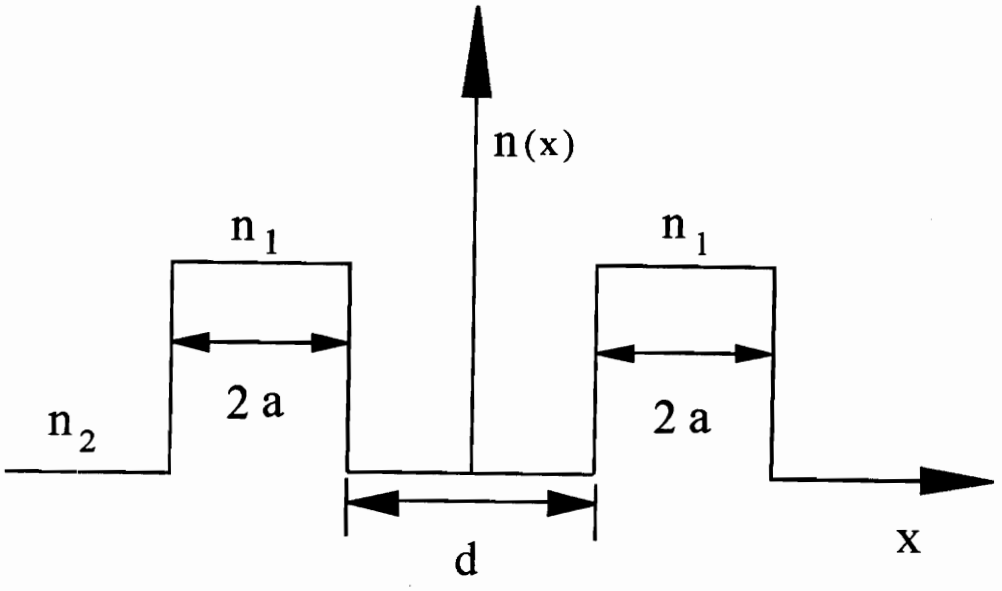

(b)

Figure 5.4: (a) Coordinates and dimensions of the identical-wavegude structure. (b) Refractive index profile of the structure.

$$\vec{e}_{1t}^{(1)}(x) = \begin{cases} P\cos(U)\ \exp[W/a(a-x)]\,\vec{a}_y, & x \geq a \\ P\cos(Ux/a)\,\vec{a}_y, & |x| \leq a \\ P\cos(U)\ \exp[W/a(a+x)]\,\vec{a}_y, & x \leq -a \end{cases} \tag{5.37}$$

$$\vec{e}_{1t}^{(2)}(x) = \begin{cases} P\cos(U)\ \exp[W/a(a-x')]\,\vec{a}_y, & x' \geq a \\ P\cos(Ux'/a)\,\vec{a}_y, & |x'| \leq a \\ P\cos(U)\ \exp[W/a(a+x')]\,\vec{a}_y, & x' \leq -a \end{cases} \tag{5.38}$$

where

$$x' = x - (2a+d) \tag{5.39}$$

$$P = \sqrt{\frac{2\omega\mu W}{\beta a(1+W)}} \tag{5.40}$$

$$U = a\sqrt{k_0^2\, n_1^2 - \beta^2} \tag{5.41}$$

$$W = a\sqrt{\beta^2 - k_0^2\, n_2^2} \tag{5.42}$$

$$k_0 = \frac{2\pi}{\lambda_0}, \tag{5.43}$$

$\vec{a}_y$ is the unit vector in the y-direction and λ_0 is the free-space wavelength. The coefficient P defined in equation (5.40) serves to normalize the modal fields. The propagation constant β in the above equations is for the TE_0 mode in a single guide in isolation and can be determined using the characteristic equation derived from the continuity of tangential fields [29]

$$U = \arctan\left(\frac{W}{U}\right). \tag{5.44}$$

Substituting equations (5.37) and (5.38) into equation (2.17) and performing the integration, the coupling coefficient k is obtained as

$$k = \frac{U^2 W^2 \exp(-Wd/a)}{\beta a^2 V^2 (W+1)}, \tag{5.45}$$

where

$$V = \sqrt{U^2 + W^2} = ak_0\sqrt{n_1^2 - n_2^2}\,. \tag{5.46}$$

For a given guide, if the wavelength (i.e., $\lambda_0 = 2\pi/k_0$) is known, the propagation constant β can be obtained from equation (5.44). Having obtained k_0 and β, the coupling coefficient k is uniquely determined from (5.45).

5.2 Structure with Nonidentical Guides

The formulation of Section 5.1 is extended to the nonidentical waveguide case. As already discussed in Chapter 3, nonidentical waveguide structures can take advantage of the phase mismatch between the guides to enhance wavelength discrimination capability. Thus, nonidentical waveguide structures are expected to have more improved spectral responses, especially when they are used as narrow wavelength filters.

5.2.1 Cavity Resonator

The procedure for determining the resonance conditions is the same as that for the identical waveguides case. Only the calculations are more complicated. From the solutions of coupled-mode equations in (3.1) and (3.2), we can obtain the following relations between amplitude coefficients of forward and backward traveling waves at end points

$$A_1(L) = Z_1\,A_1(0) + Z_2\,A_2(0) \tag{5.47}$$

$$A_2(L) = Z_3\,A_1(0) + Z_4\,A_2(0), \tag{5.48}$$

and

$$B_1(L) = Z_1\,B_1(0) + Z_2\,B_2(0) \tag{5.49}$$

$$B_2(L) = Z_3\,B_1(0) + Z_4\,B_2(0), \tag{5.50}$$

where

$$
\begin{aligned}
Z_1 &= \frac{s+\delta}{2s}\exp\left[-j(s-\delta)L\right] + \frac{s-\delta}{2s}\exp\left[j(s+\delta)L\right] \\
Z_2 &= \frac{k_{12}}{2s}\left\{\exp\left[-j(s-\delta)L\right] - \exp\left[j(s+\delta)L\right]\right\} \\
Z_3 &= -\frac{k_{21}}{k_{12}}\,Z_2^* \\
Z_4 &= Z_1^*,
\end{aligned}
$$

with s given by equation (3.8). In addition, four boundary conditions from the continuity of tangential components of fields at the perfect mirrors are given by

$$A_1(0) = -B_1(L)\,e^{-j\beta_1 L} \tag{5.51}$$

$$A_2(0) = -B_2(L)\,e^{-j\beta_2 L} \tag{5.52}$$

$$B_1(0) = -A_1(L)\,e^{-j\beta_1 L} \tag{5.53}$$

$$B_2(0) = -A_2(L)\,e^{-j\beta_2 L}, \tag{5.54}$$

where β_1 and β_2 are the propagation constants of individual guides in isolation. The terms k_{11} and k_{22} described in (2.20) and (2.21) are neglected. We have assumed here that the waveguides are lossless.

To have a nontrivial solution for the eight simultaneous equations (6.1)-(6.8), it is required that

$$
\begin{aligned}
\frac{A_1(0)}{A_2(0)} &= \frac{Z_1 Z_2\, e^{-j2\beta_1 L} + Z_2 Z_4\, e^{-j(\beta_1+\beta_2)L}}{1 - \left[\, Z_1^2\, e^{-j2\beta_1 L} + Z_2 Z_3\, e^{-j(\beta_1+\beta_2)L}\,\right]} \\
&= \frac{1 - \left[\, Z_4^2\, e^{-j2\beta_2 L} + Z_2 Z_3\, e^{-j(\beta_1+\beta_2)L}\,\right]}{Z_3 Z_4\, e^{-j2\beta_1 L} + Z_1 Z_3\, e^{-j(\beta_1+\beta_2)L}}.
\end{aligned} \tag{5.55}
$$

After some manipulation, equation (5.55) can be reduced to

$$\exp\left[j(\beta_1+\beta_2)L\right] + \exp\left[-j(\beta_1+\beta_2)L\right] = \exp(j2sL) + \exp(-j2sL). \tag{5.56}$$

Again, two sets of solutions can satisfy equation (5.56). They are

$$(\beta_1 + \beta_2)\, L = -2sL + 2m\pi \qquad m = 1, 2, 3, \ldots \tag{5.57}$$

$$(\beta_1 + \beta_2)\, L = 2sL + 2n\pi \qquad n = 1, 2, 3, \ldots, \tag{5.58}$$

or equivalently,

$$\beta_e L = m\pi \tag{5.59}$$

$$\beta_o L = n\pi, \tag{5.60}$$

where β_e and β_o, defined in (3.9) and (3.10), are the propagation constants of the two fundamental modes of the coupled-waveguide structure.

Equations (5.59) and (5.60) demonstrate once more that the resonance conditions of the composite waveguide resonator structure amount to the condition that the two fundamental modes be at resonance simultaneously.

5.2.2 Wavelength Filter

For the nonidentical coupled-waveguide F-P filter, the boundary conditions are given by

$$A_1(0) = B_1(L)e^{-j\beta_1 L}\, r_1 \tag{5.61}$$

$$A_2(0) = B_2(L)e^{-j\beta_2 L}\, r_1 + (1 - r_1)E_i \tag{5.62}$$

$$B_1(0) = A_1(L)e^{-j\beta_1 L}\, r_2 \tag{5.63}$$

$$B_2(0) = A_2(L)e^{-j\beta_2 L}\, r_2. \tag{5.64}$$

Solving equation (5.47)-(5.50) and (5.61)-(5.64) for $A_1(L)$ and $A_2(L)$, we obtain

$$A_1(L) = \frac{E_i}{DEN}\, \{Z_2(1 - r_1)(1 + r_1 r_2 \exp[-j(\beta_1 + \beta_2)L]\} \tag{5.65}$$

$$A_2(L) = \frac{E_i}{DEN}\, [Z_4 - Z_1 r_1 r_2 \exp(-j2\beta_1 L)], \tag{5.66}$$

where

$$DEN = 1 - 2Z_2Z_3r_1r_2\,e^{-j(\beta_1+\beta_2)L} - r_1r_2\left[Z_1^2\,e^{-j2\beta_1L} + Z_4^2\,e^{-j2\beta_2L}\right] + r_1^2r_2^2\left(Z_1Z_4 - Z_2Z_3\right)^2 e^{-j2(\beta_1+\beta_2)L}.$$

The output amplitudes from the two guides are given by

$$E_{out1} = A_1(L)e^{-j\beta_1L}(1+r_2) \tag{5.67}$$

$$E_{out2} = A_2(L)e^{-j\beta_2L}(1+r_2). \tag{5.68}$$

The transmittance of each guide can be obtained by combining (5.65)-(5.68). They are calculated as

$$\mathcal{T}_1(f) = \left|\frac{E_{out1}}{E_i}\right|^2 = \frac{(1+r_2)^2(1-r_1)^2\,k_{12}^2}{4s^2}\left|\frac{e^{-j\beta_eL}}{1-r_1r_2\,e^{-j2\beta_eL}} - \frac{e^{-j\beta_oL}}{1-r_1r_2\,e^{-j2\beta_oL}}\right|^2 \tag{5.69}$$

$$\mathcal{T}_2(f) = \left|\frac{E_{out2}}{E_i}\right|^2 = \frac{(1+r_2)^2(1-r_1)^2}{4s^2}\left|\frac{(s-\delta)\,e^{-j\beta_eL}}{1-r_1r_2\,e^{-j2\beta_eL}} + \frac{(s+\delta)\,e^{-j\beta_oL}}{1-r_1r_2\,e^{-j2\beta_oL}}\right|^2. \tag{5.70}$$

By letting the two guides become identical, $\delta = 0, s = k_{12} = k_{21} = k$, and equations (5.69) and (5.70) should be and are indeed reduced to (5.35) and (5.36). This is a check on the validity of equations (5.69) and (5.70). As described in the identical waveguide case, $\mathcal{T}_2 = 1$ implies 100% transmittance (if $r_1 = r_2 \equiv r$). $\mathcal{T}_1$ is zero when resonance conditions (5.59) and (5.60) are satisfied, and m, n are both even or both odd and phase is matched for the two guides. However, if either m or n is even and the other is odd, the transmittance $\mathcal{T}_1$ is not 100% and $\mathcal{T}_2$ is not zero but that

$$\mathcal{T}_1(f) = \frac{(1-r^2)^2\,k_{12}^2}{4s^2}\left|\frac{1}{1-r^2} + \frac{1}{1-r^2}\right|^2 = \left(\frac{k_{12}}{s}\right)^2 \tag{5.71}$$

$$\mathcal{T}_2(f) = \frac{(1-r^2)^2}{4s^2}\left|\frac{s-\delta}{1-r^2} - \frac{s+\delta}{1-r^2}\right|^2 = \left(\frac{\delta}{s}\right)^2. \tag{5.72}$$

Equations (5.71) and (5.72) reinforce the fact that complete transfer of power cannot be achieved in the case of nonidentical waveguides because of the phase mismatch. The larger the phase mismatch δ, the more power remains in guide 2 and less power is transferred to guide 1. As we can see, the main feature of the directional coupler filter is incorporated in this coupled-guide resonator filter.

5.2.3 Coupling Coefficients, k_{12} and k_{21}

Although for nonidentical parallel waveguides more accurate analysis should include the overlap integral, since our interest here is not in the accuracy of couple-mode theory but in utilizing this theory as a tool, for simplicity, we neglect the overlap integral $\bar{C}$ in equations (2.34) and (2.35) and use them as quantities for the coupling coefficients. In addition, the modified propagation constants γ_1 and γ_2 in coupled-mode equations are approximated by β_1 and β_2, propagation constants of TE_0 mode of each guide in isolation. Thus, the coupling coefficients are given by

$$k_{uv} = \tilde{k}_{uv} = \frac{\omega\epsilon_0}{4}\int_{-\infty}^{\infty} (n_c^2 - n_v^2)\, \vec{e}_{1t}^{(u)} \cdot \vec{e}_{1t}^{(v)}\, dx \qquad u, v = 1, 2. \tag{5.73}$$

The last term in (2.29) which includes $e_{1z}^{(1)}$ and $e_{1z}^{(2)}$ is discarded because we assume the guided modes are TE polarized. The transverse fields $\vec{e}_{1t}^{(1)}$ and $\vec{e}_{1t}^{(2)}$, referred to the nonidentical waveguides configuration in Figure 5.5, are similar to (5.37) and (5.38). Performing the integration in (5.73) yields

$$k_{uv} = \frac{k_0^2(n_v^2 - n_3^2)}{2\sqrt{\beta_1\beta_2 a_1 a_2}} \sqrt{\frac{W_1 W_2}{(1+W_1)(1+W_2)}}\, \cos(U_u)\, e^{-\frac{W_u}{a_u}(a_v+d)}\, I_{uv}\,, \tag{5.74}$$

where

$$\begin{aligned} I_{uv} &= \frac{2a_1a_2}{U_v^2 + W_u^2}\left[\, a_u U_v \sin(U_v)\cosh(W_u a_v/a_u) + a_v W_u \cos(U_v)\sinh(W_u a_v/a_u)\,\right] \\ U_i &= a_i\sqrt{k_0^2\, n_i^2 - \beta_i^2} \\ W_i &= a_i\sqrt{\beta_i^2 - k_0^2\, n_i^2} \qquad u, v, i = 1, 2. \end{aligned}$$

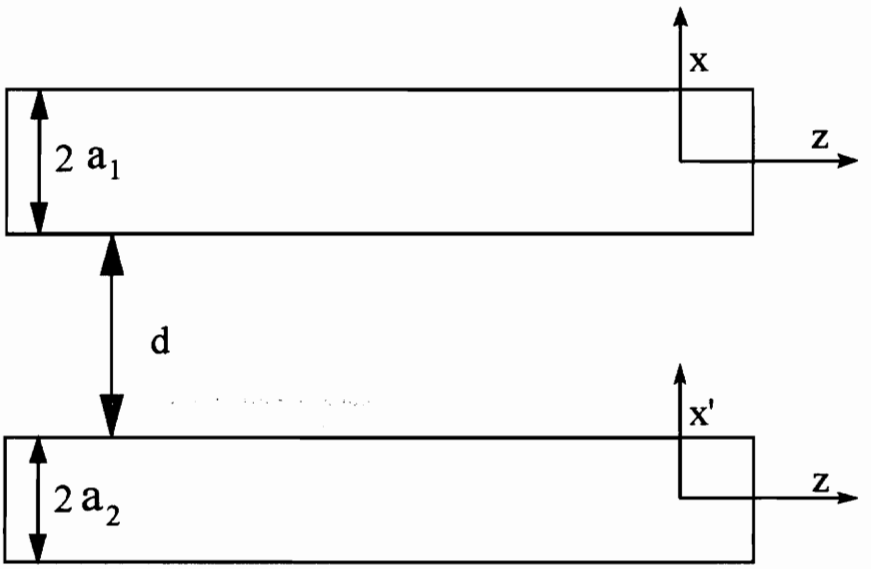

(a)

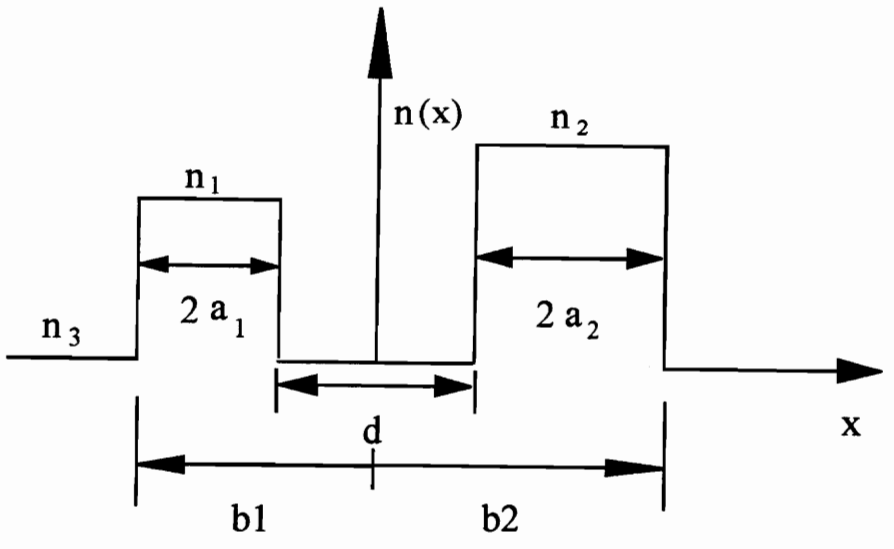

(b)

Figure 5.5: (a) Coordinates and dimensions of the nonidentical-wavegude structure. (b) Refractive index profile of the structure.

The constants β_1 and β_2 can be obtained from the characteristic equation of each guide in isolation.

5.3 Comparison of Propagation Constants from Coupled-Mode and Exact Analyses

This section is devoted to investigating the accuracy of our coupled-mode formulation described in the previous section. The propagation constants of the two guided modes, β_e and β_o, derived from coupled-mode theory, are compared with the exact solutions of a two-dimentional composite waveguide structure.

5.3.1 Identical-Waveguide Case

The exact propagation constants of the first two TE modes, denoted as β_{TE0} and β_{TE1}, can be uniquely determined from the characteristic equation. The propagation constants β_e and β_o derived from coupled-mode theory are now compared to β_{TE0} and β_{TE1} for the waveguide structure shown in Figure 5.4 with parameters chosen as: $n_1 = 3.56$, $n_2 = 1.45$, $a = 0.1\ \mu m$, $d = 0.1$, and $0.3\ \mu m$. Figure 5.6 (a) with $d = 0.3\ \mu m$ shows that the β_e and β_o agree very well with β_{TE0} and β_{TE1}. The errors of the coupled-mode results are within 0.03% for this configuration. As the distance between the two guides d decreases, the coupling effect increases and the coupled-mode solution becomes less accurate. When d reduces to 0.1, Figure 5.6 (b) shows that the coupled-mode results deviate farther away from the exact solutions than those in Figure 5.6 (a). The errors for $d = 0.1\ \mu m$ case are about 0.7%.

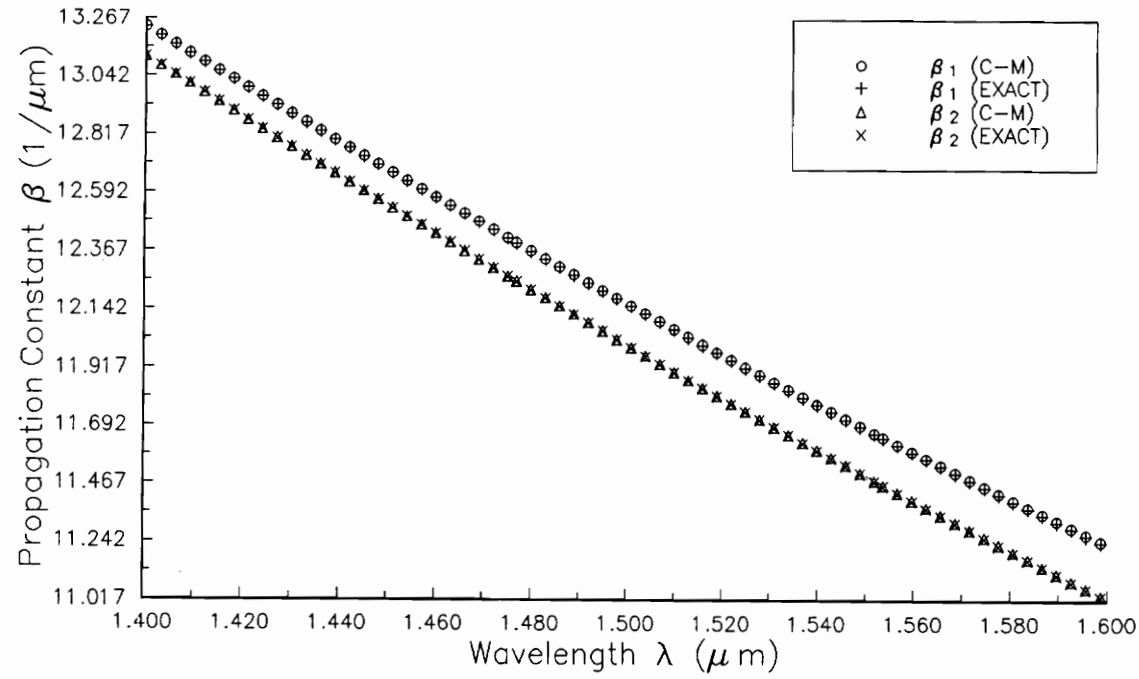

(a)

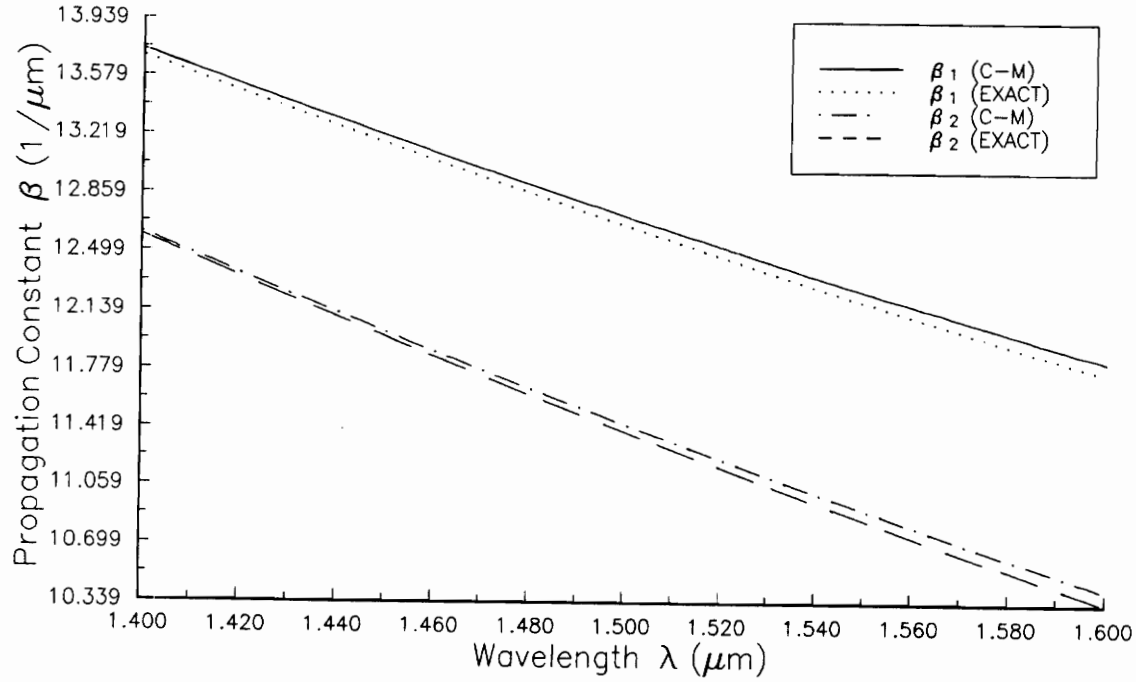

(b)

Figure 5.6: Comparison of propagation constants from coupled-mode and exact analyses. Identical-waveguide structure with $n_1 = 3.56$, $n_2 = 1.45$, $a = 0.1\ \mu m$. (a) $d = 0.3\ \mu m$; (b) $d = 0.1\ \mu m$.

5.3.2 Nonidentical-Waveguide Case

The nonidentical waveguides structure with an index profile shown in Figure 5.5 is a five-layer asymmetric slab guide. The propagation constants β_{TE0} and β_{TE1} are the first two roots of β of the characteristic equation for TE modes. The propagation constants β_e and β_o from the coupled-mode theory for the asymmetrical waveguides are given in (3.9) and (3.10). With the aid of equations (5.44) (for β_1, β_2) and (6.28) (for k_{12}, k_{21}), β_e and β_o can be readily obtained. Figure 5.7 (a) demonstrates that coupled-mode results are accurate within 0.03% for the case of $d = 0.3\ \mu m$ (weaker coupling). For the stronger coupling case of $d = 0.1\ \mu m$ the results are less accurate with errors within 0.8%, as shown in Figure 5.7 (b).

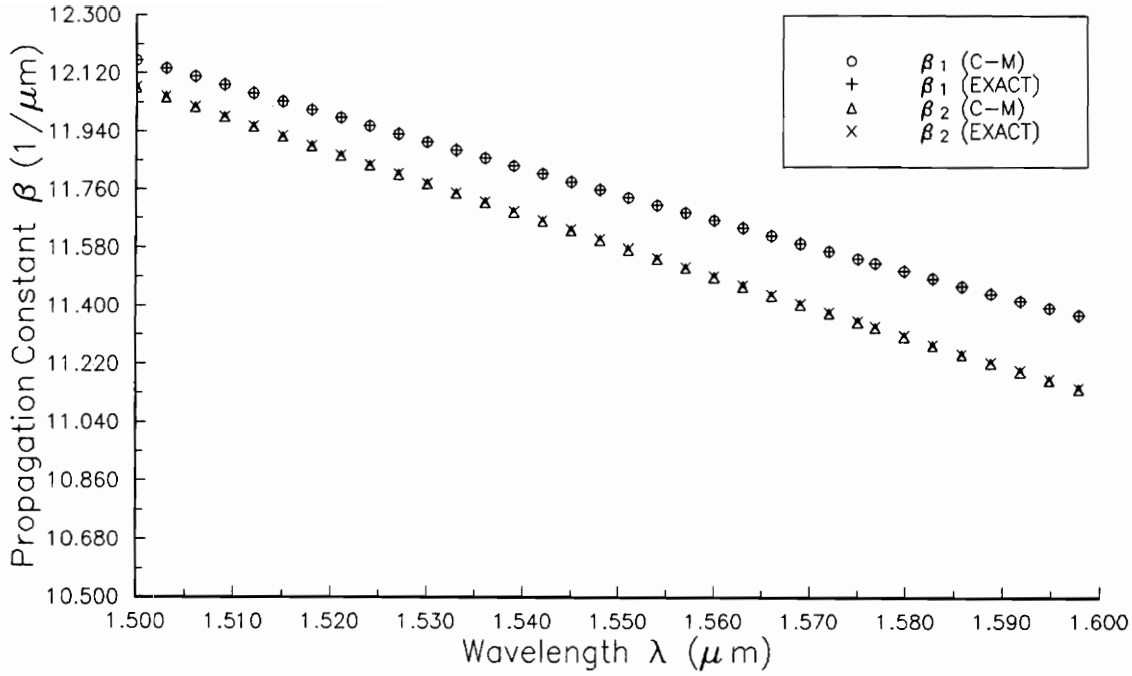

(a)

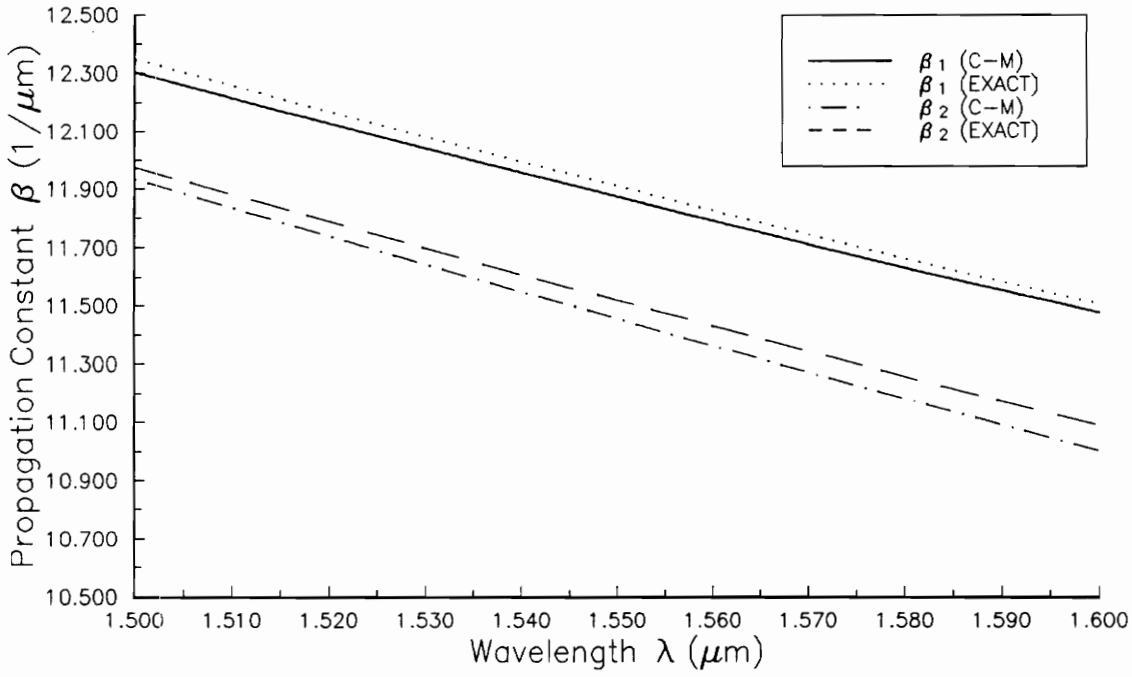

(b)

Figure 5.7: Comparison of propagation constants from coupled-mode and exact analyses. Nonidentical-waveguide structure with $n_1 = 3.56$, $n_2 = 3.0$, $n_3 = 1.45$, $a_1 = 0.1\ \mu m$, and $a_2 = 0.4\ \mu m$. (a) $d = 0.3\ \mu m$; (b) $d = 0.1\ \mu m$.

Chapter 6

Numerical Results

In this chapter, numerical results based on the formulations developed in Chapter 5 are presented. Spectral characteristics of the proposed coupled-waveguide F-P resonators for several example cases are calculated and discussed. The effects of various parameters, such as refractive indices of the layers, cavity length, and reflection coefficients of end mirrors, are investigated.

6.1 Identical-Waveguide Case

Equations (5.35) and (5.36) are used to generate the numerical results. They can be rewritten as

$$\mathcal{T}_1(f) = \left|\frac{E_{out1}}{E_i}\right|^2$$

$$= \sin^2(kL)\cdot(1-r^2)^2 \left|\frac{r^2 + e^{j2\beta L}}{r^4\, e^{-j4\beta L} + e^{j2\beta L} - 2r^2\cos(2kL)}\right|^2 \tag{6.1}$$

$$\mathcal{T}_2(f) = \left|\frac{E_{out2}}{E_i}\right|^2$$

$$= \cos^2(kL)\cdot(1-r^2)^2 \left|\frac{r^2 - e^{-j2\beta L}}{r^4\, e^{-j4\beta L} + e^{j2\beta L} - 2r^2\cos(2kL)}\right|^2, \qquad (6.2)$$

where r_1 and r_2 are both set equal to r. The factors $\sin^2(kL)$ and $\cos^2(kL)$ in (6.1) and (6.2) show that the coupled-waveguide F-P structure incorporates the power transfer characteristics of the directional coupler given in equations (3.20) and (3.21). In fact, by letting $r = 0$ (6.1) and (6.2) reduce to (3.20) and (3.21), respectively. If $\sin^2(kL) = 1$ ($2kL = p\pi$, p being an odd integer) and $\exp(2\beta L) = -1$ ($2\beta L = q\pi$, q being an odd integer) , $\mathcal{T}_1(f) = 1$ and light launched (or generated) in guide 2 is coupled to guide 1 completely. This corresponds to one of the resonance conditions described in equations (5.20) and (5.21). The case of both p and q being even integers corresponds the other resonance condition which makes $\mathcal{T}_2(f) = 1$ and $\mathcal{T}_1(f) = 0$. Here attention is focused only on $\mathcal{T}_1(f)$. Discussion of $\mathcal{T}_2(f)$ is similar.

As shown in (6.1), the transmission spectrum $\mathcal{T}_1(f)$ is explicitly a function of k, β, L and r. However, k and β are determined by the index profile of the coupled-waveguide structure. Figure 6.1 shows the transmittance characteristic of a filter with parameters, referred to Figure 5.4, $n_1 = 3.56$, $n_2 = 1.45$, $a = 0.1\ \mu m$, $L = 300\ \mu m$ and $r = 0.9$. A main resonance with almost unity transmission occurs at a wavelength around $1.55\ \mu m$. Figure 6.1 (b) illustrates the details of the transmission characteristic in a very narrow spectral range. The dashed line in Figure 6.1 (a) shows the trace of $\sin^2(kL)$. As already mentioned, maximum transmission occurs when $\sin^2(kL) = 1$ and $\exp(2\beta L) = -1$. Since propagation constant β is always much larger than coupling coefficient k, the occurrence of the condition $\exp(2\beta L) = -1$ is much more frequent than that of $\sin^2(kL) = 1$. Therefore, though at every point where $\sin^2(kL) = 1$ the condition $\exp(2\beta L) = -1$ is not usually exactly satisfied, the

next wavelength which matches the condition $\exp(2\beta L) = -1$ is very close to the peaks of $\sin^2(kL)$. The wavelengths 1.535 μm and 1.566 μm in Figure 6.1 (a) are such points. At these wavelengths the transmission is significant but not maximum. The magnitude of transmission depends on how far these points are from the peaks of $\sin^2(kL)$. By slightly adjusting the length of the structure, maximum transmission at these wavelengths can occur. As illustrated in Figure 6.2, when L is changed to 299.68 μm, transmission at 1.566 μm is peaked. To design a filter at some specific wavelength, L is roughly chosen such that $\sin^2(kL) \approx 1$ at this wavelength. Then L is slightly adjusted to shift the nearest point of $\exp(2\beta L) = -1$ close to the peak of $\sin^2(kL)$.

The FWHM bandwidth of the aforementioned resonator is about 0.085 nm and the extinction ratio (the level of the first neighboring subpeak is considered as a measure of extinction ratio) is about -5.3 dB, as is more clearly seen in Figure 6.1 (b). If the distance between the two guides, d, increases, the coupling coefficient k decreases. As a result, the period of the $\sin^2(kL)$ increases while the extinction ratio decreases. As illustrated in Figure 6.3, for $d = 0.3$ μm the spacing between two consecutive peaks of $\sin^2(kL)$ is 42 nm as compared to 15 nm for the case of $d = 0.1$ μm. Also, extinction ratio is reduced to -3 dB. This behavior is somewhat similar to the three-mirror F-P resonator discussed in Chapter 4 in that as the FSR increases, the sidelobes also increase.

Figure 6.4 shows the influence of reflection coefficient on the spectral response. The characteristic in this figure corresponds to $r = 0.75$. Because the coupling coefficient k and propagation constant β are not affected by r, the envelope $\sin^2(kL)$ maintains the same shape and the main resonance still occurs at $\lambda = 1.55$ μm.

However, the FWHM bandwidth and the sidelobe level increase.

The coupled-waveguide F-P structures discussed above may serve as narrow pass-band spectral filters. However, the subpeak levels are too high for them to be fully utilized in wavelength division multiplexing. One remedy is to eliminate the periodic nature of the spectrum by making the envelope of the spectrum decay rapidly as the wavelength moves away from the desired main resonance wavelength. Non-identical waveguide structures exhibit this kind of characteristic by means of the phase mismatch between the two guides. We will discuss more about this issue in a later section. Another way to reduce the sidelobes is by cascading two or more such coupled-waveguide F-P filters. If two filters with characteristics exactly the same as that in Figure 6.1 are connected in tandem, the sidelobe level will be reduced to $-11.6\ dB$, as shown in Figure 6.5.

When the coupled-waveguide F-P resonator is used as a cavity for mode selection in semiconductor lasers, one guide may serve as active region in which light is generated. The generated light is coupled into the other guide and the fields of the two guides interact. Here resonant field is assumed to be generated in guide 2 through a stimulated emission process and emits from guide 1, so equation (5.35) or (6.1) should be used to determine the spectral response.

Figures 6.6 and 6.7 show the spectral characteristics of two coupled-waveguide F-P resonators with parameters chosen such that the dominant wavelength coincides with 1550 nm and 1300 nm. These are the desired wavelengths in long distance fiber optic communications. It is observed that the main resonance at 1550 nm and 1300 nm are about 4.8 dB and 3.8 dB higher than the immediate neighboring subpeaks. Thus, in diode lasers employing these structures as the cavity resonators, if the main resonance

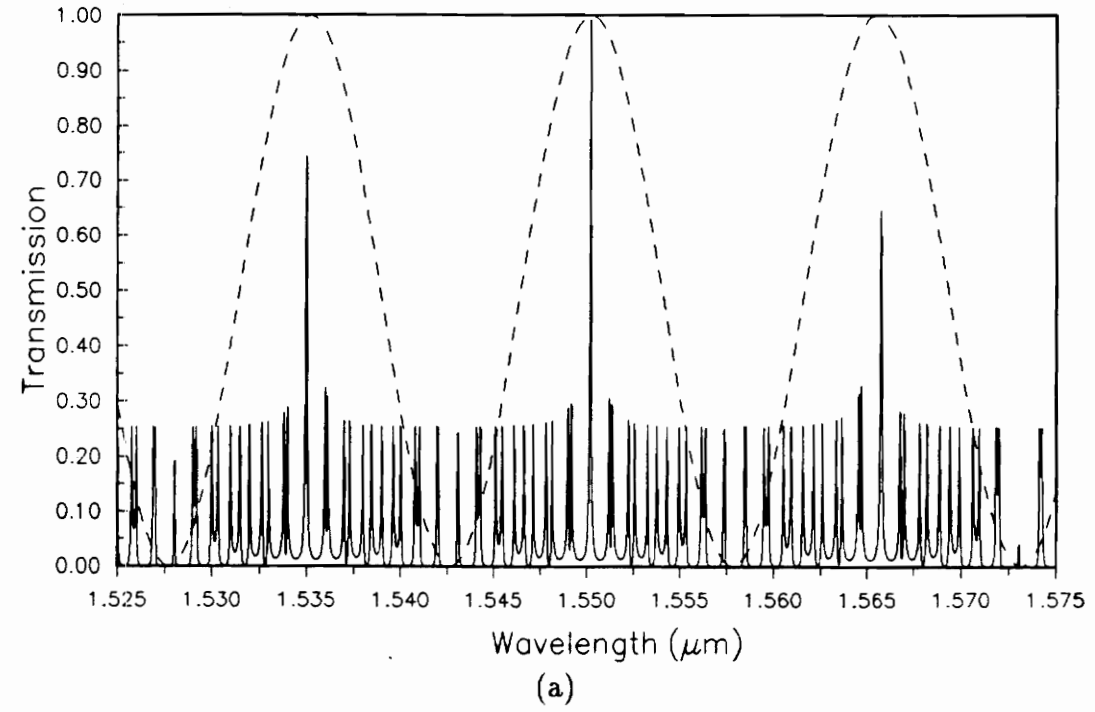

(a)

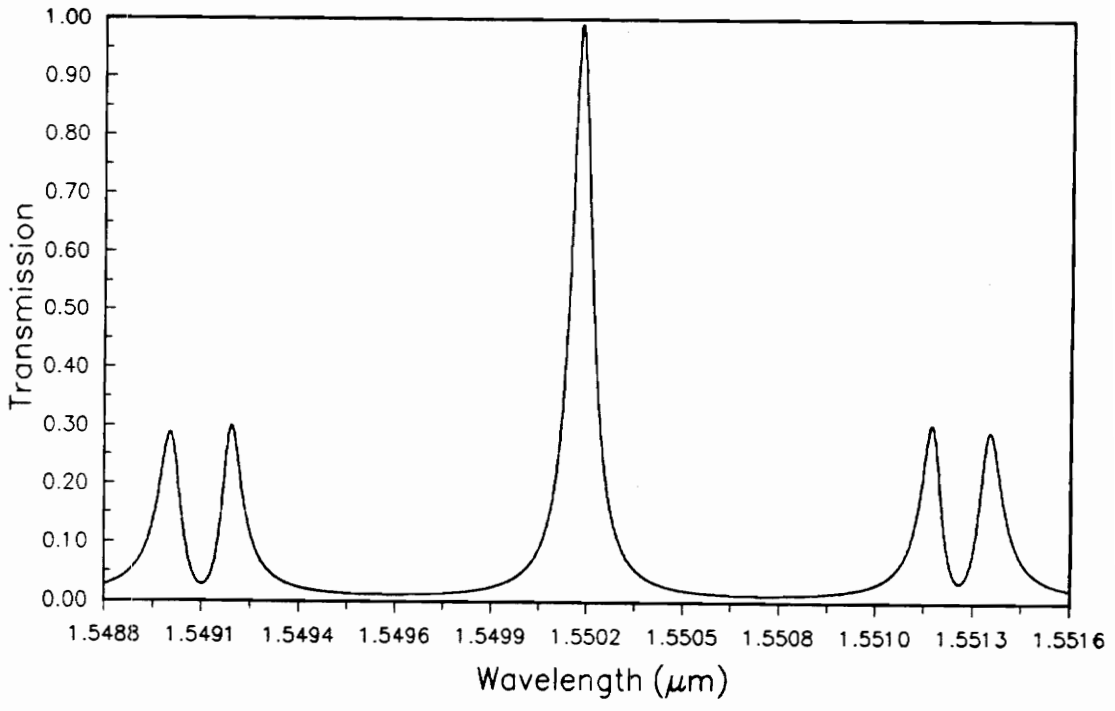

(b)

Figure 6.1: Transmittance spectrum of an identical-waveguide F-P resonator with parameters $n_1 = 3.56$, $n_2 = 1.45$, $a = 0.1\ \mu m$, $d = 0.1\ \mu m$, $L = 300.0\ \mu m$ and $r = 0.9$. (a) For $1525\ nm < \lambda < 1575\ nm$;(b) for $1548.8\ nm < \lambda < 1551.6\ nm$.

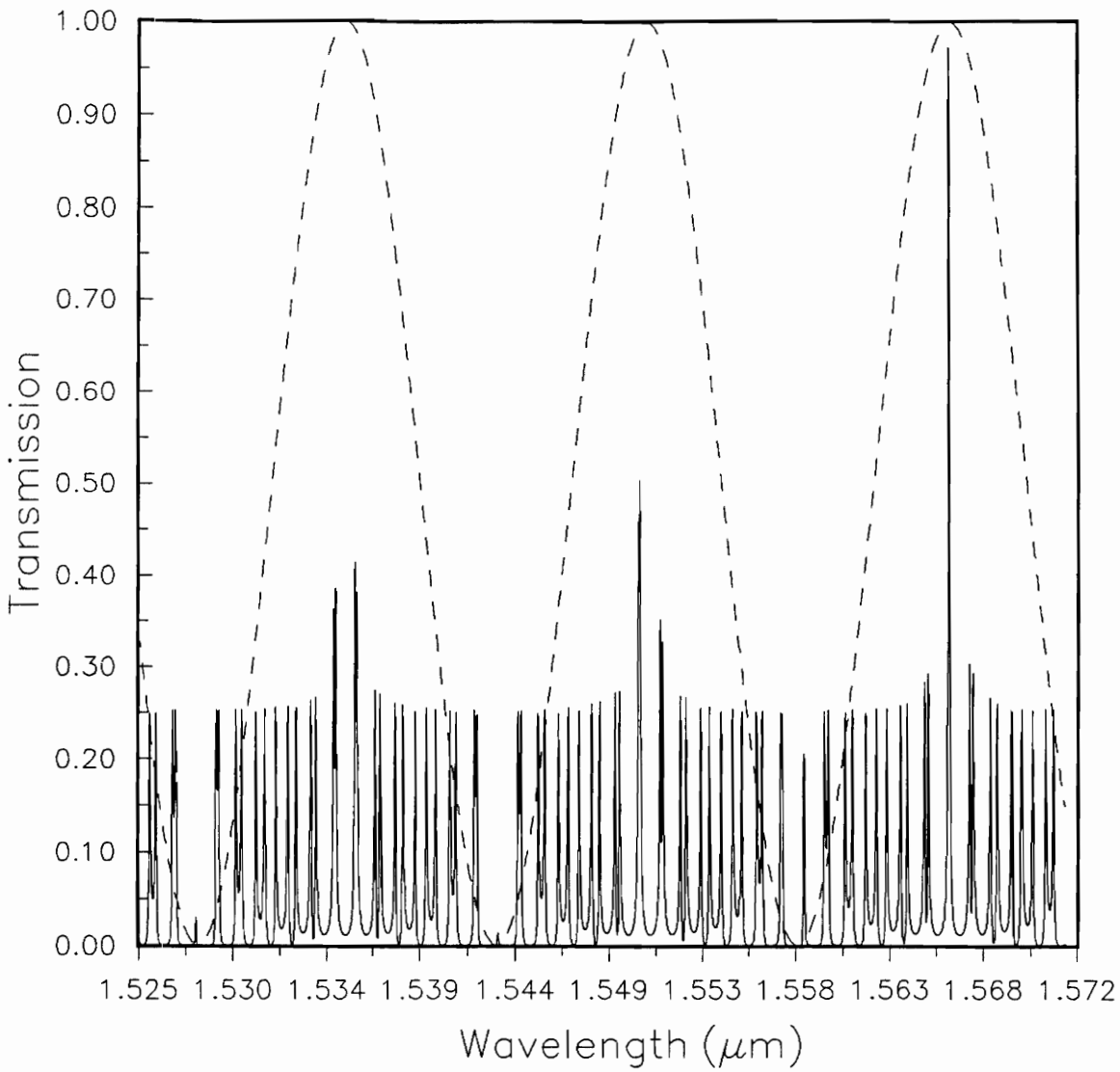

Figure 6.2: Transmittance spectrum of an identical-waveguide F-P resonator with parameters $n_1 = 3.56$, $n_2 = 1.45$, $a = 0.1\ \mu m$, $d = 0.1\ \mu m$, $L = 299.68\ \mu m$ and $r = 0.9$. Main resonance occurs at $\lambda = 1566\ nm$

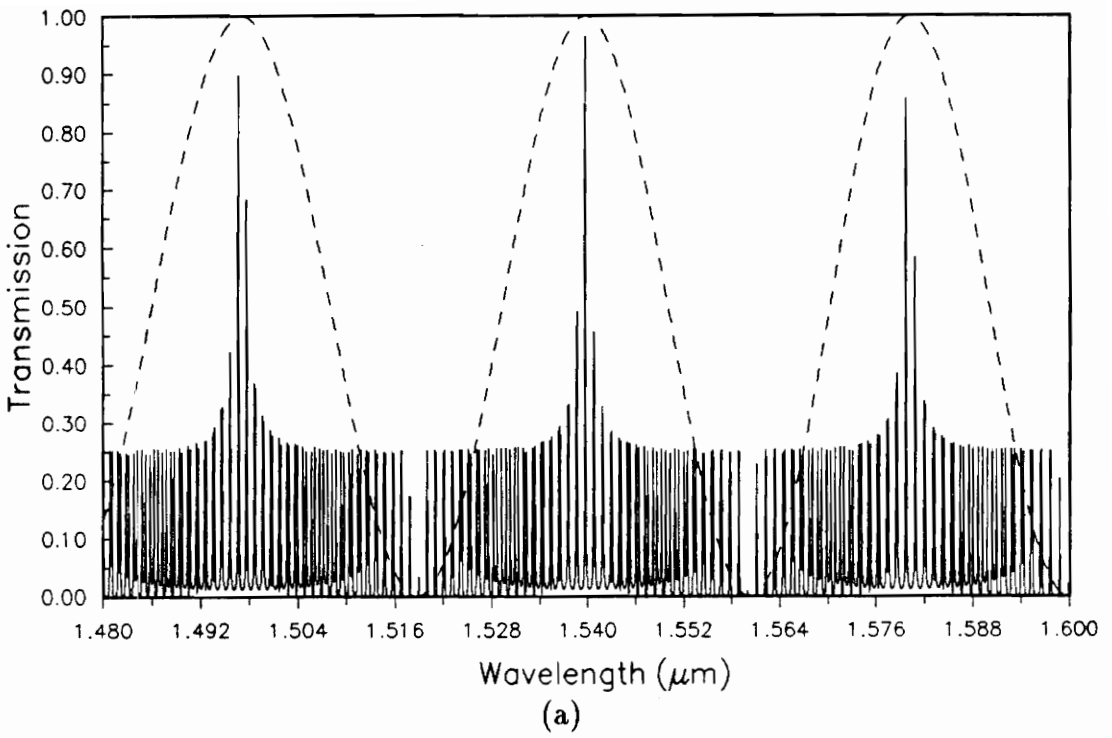

(a)

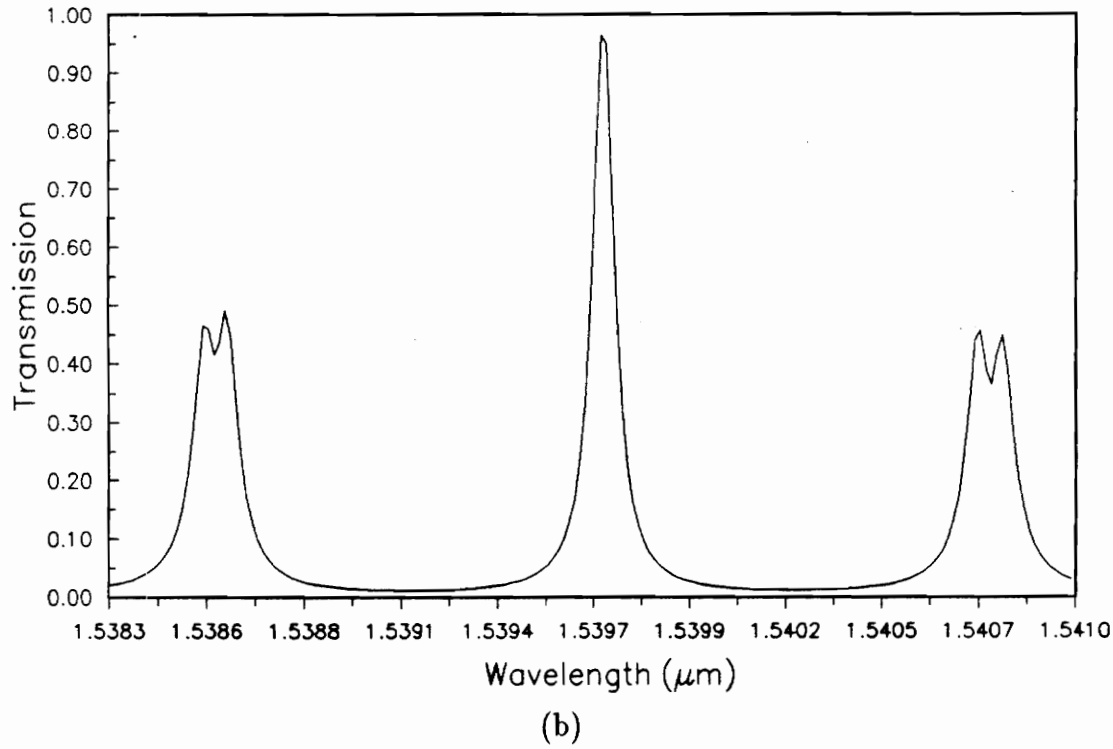

(b)

Figure 6.3: Transmittance spectrum of an identical-waveguide F-P resonator with parameters $n_1 = 3.56$, $n_2 = 1.45$, $a = 0.1\ \mu m$, $d = 0.3\ \mu m$, $L = 300.0\ \mu m$ and $r = 0.9$. (a) For $1480\ nm < \lambda < 1600\ nm$;(b) for $1538.3\ nm < \lambda < 1541.0\ nm$.

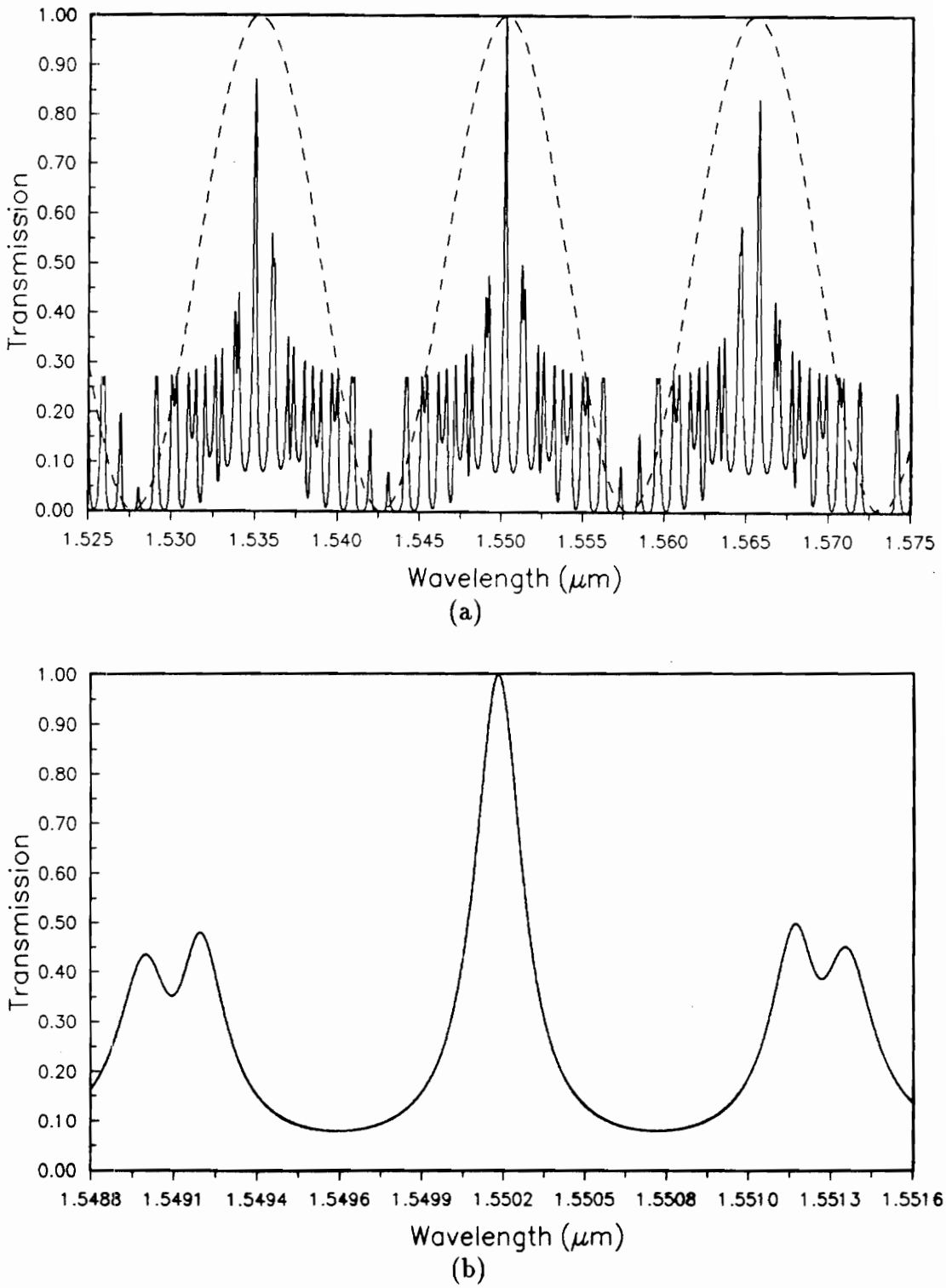

Figure 6.4: Transmittance spectrum of an identical-waveguide F-P resonator with parameters $n_1 = 3.56$, $n_2 = 1.45$, $a = 0.1\ \mu m$, $d = 0.1\ \mu m$, $L = 300.0\ \mu m$ and $r = 0.75$. (a) For $1525\ nm < \lambda < 1575\ nm$;(b) for $1548.8\ nm < \lambda < 1551.6\ nm$.

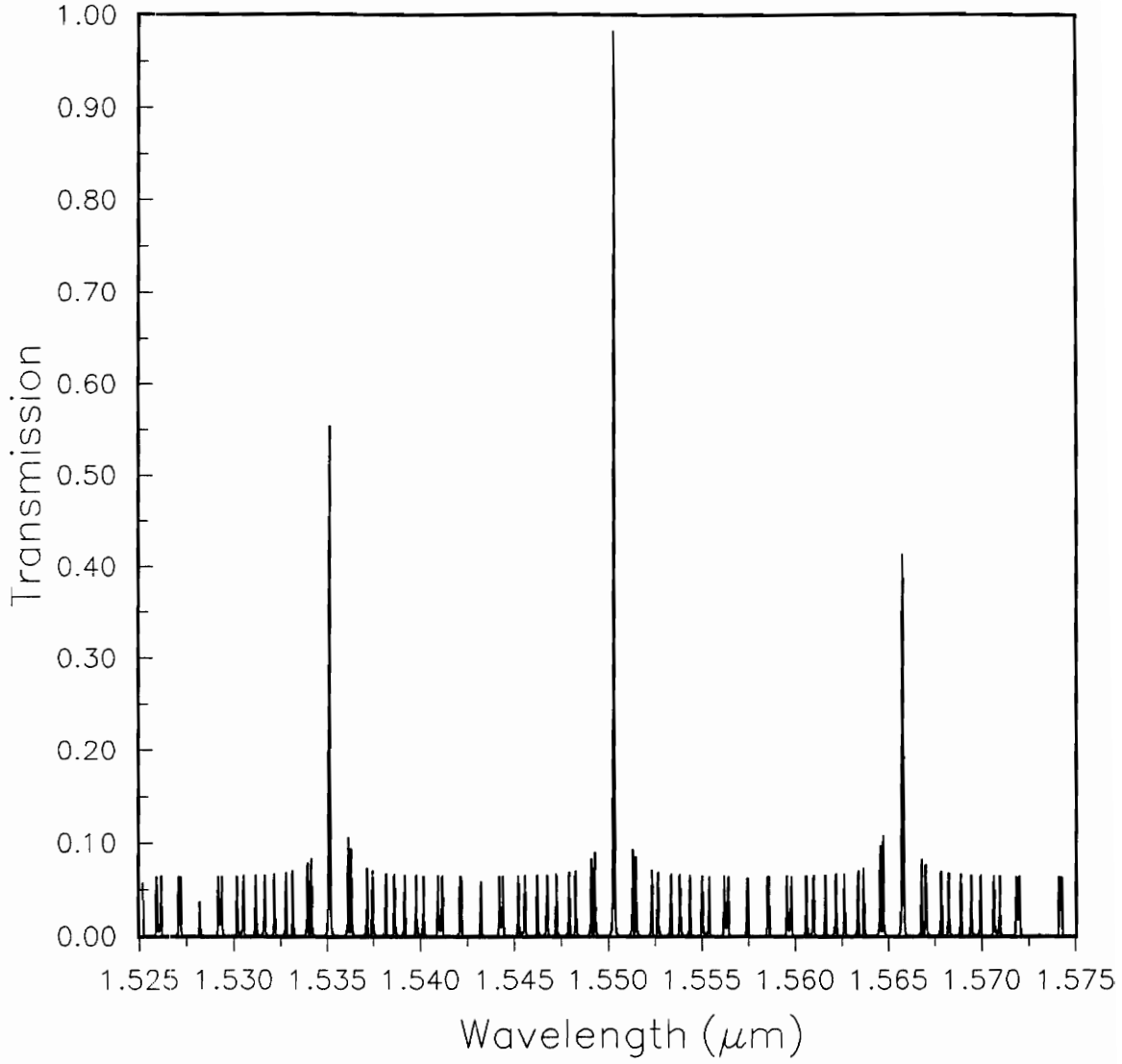

Figure 6.5: Transmission spectrum of a two-stage coupled-waveguide F-P resonator. Parameters for both stages are $n_1 = 3.56$, $n_2 = 1.45$, $a = 0.1\ \mu m$, $d = 0.1\ \mu m$, $L = 300.0\ \mu m$ and $r = 0.95$.

coincides with the peak gain profile, stimulated emission occurs predominantly at 1550 nm (or 1300 nm) and the neighboring resonant wavelengths are much less likely to be emitted. Consequently, the mode selectivity of the diode laser is enhanced and its spectral purity is improved. In diode lasers with conventional single-guide F-P resonators, the neighboring resonant wavelengths have the same peak and only the gain profile will cause one mode to dominate over the rest; thus the possibility of mode jumping and frequency instability.

6.2 Nonidentical-Waveguide Case

Similar to the identical-waveguide case, the transmission function of waveguide 1 given in equation (5.69) can be rewritten as

$$\begin{aligned} \mathcal{T}_1(f) &= \left|\frac{E_{out1}}{E_i}\right|^2 \\ &= \frac{k_{12}^2}{s^2}\sin^2(sL)\cdot(1-r^2)^2\left|\frac{r^2+e^{j2\bar{\beta}L}}{r^4\,e^{-j4\bar{\beta}L}+e^{j2\bar{\beta}L}-2r^2\cos(2sL)}\right|^2, \end{aligned} \tag{6.3}$$

where

$$s = \sqrt{k_{12}k_{21}+\delta^2} \tag{6.4}$$

$$\bar{\beta} = \frac{\beta_1+\beta_2}{2}. \tag{6.5}$$

Again, the factor $(k_{12}^2/s^2)\sin^2(sL)$ describes a behavior attributed to directional couplers. The procedure for optimizing the transmission spectrum is more complicated in the nonidentical-waveguide case. First, the parameters n_1, n_2, n_3, a_1 and a_2, indicated in Figure 5.5, have to be chosen such that the phase-matched point is at the desired wavelength. Then the length L is decided such that $\sin^2(sL) = 1$ at the phase-matched point in order to have a complete transfer of power.

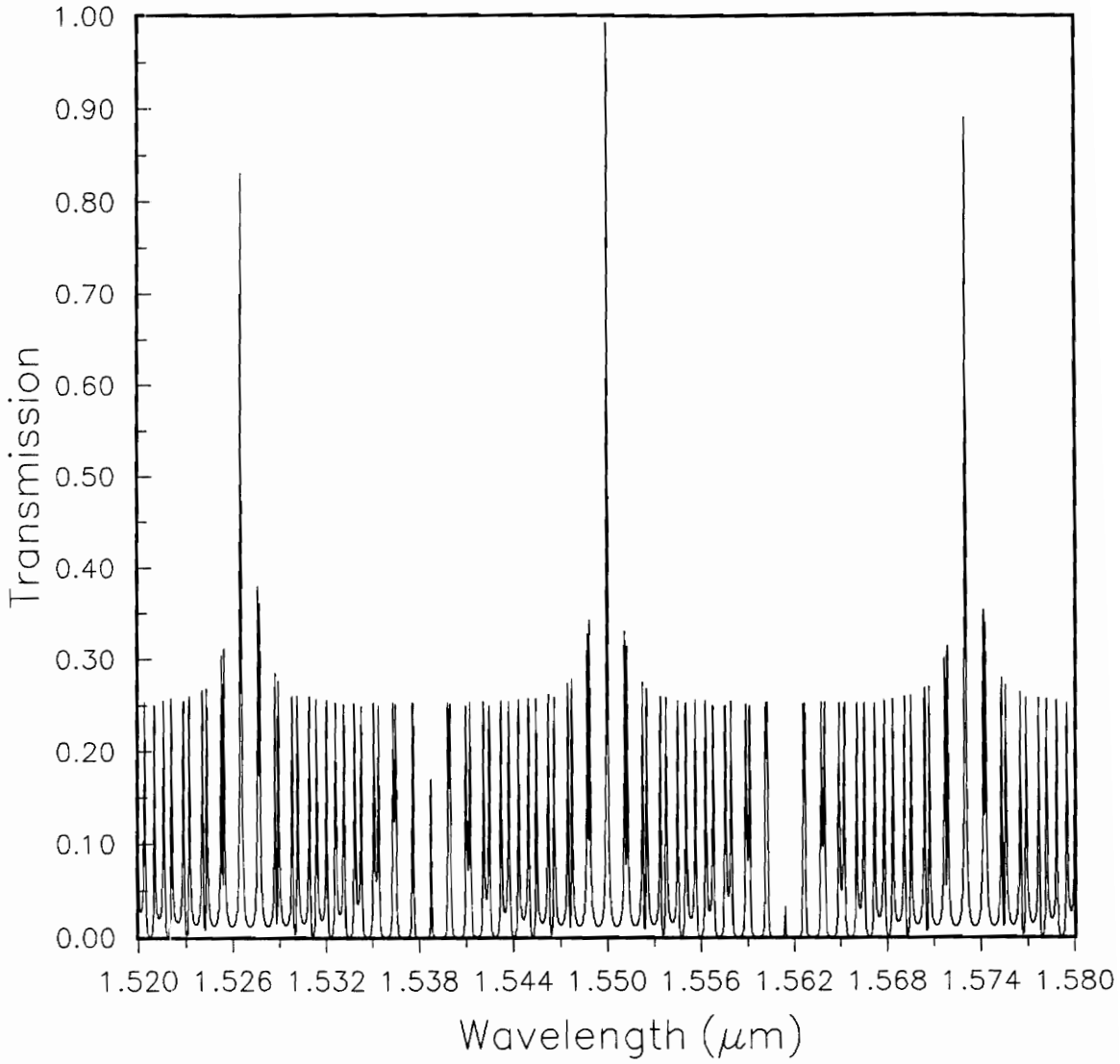

Figure 6.6: Spectral characteristic of cavity resonator of with peak transmission at 1550 nm. Parameters are $n_1 = 3.77$, $n_2 = 3.2$, $a = 0.08\ \mu m$, $d = 0.07\ \mu m$, $L = 296.47\ \mu m$ and $r = 0.9$.

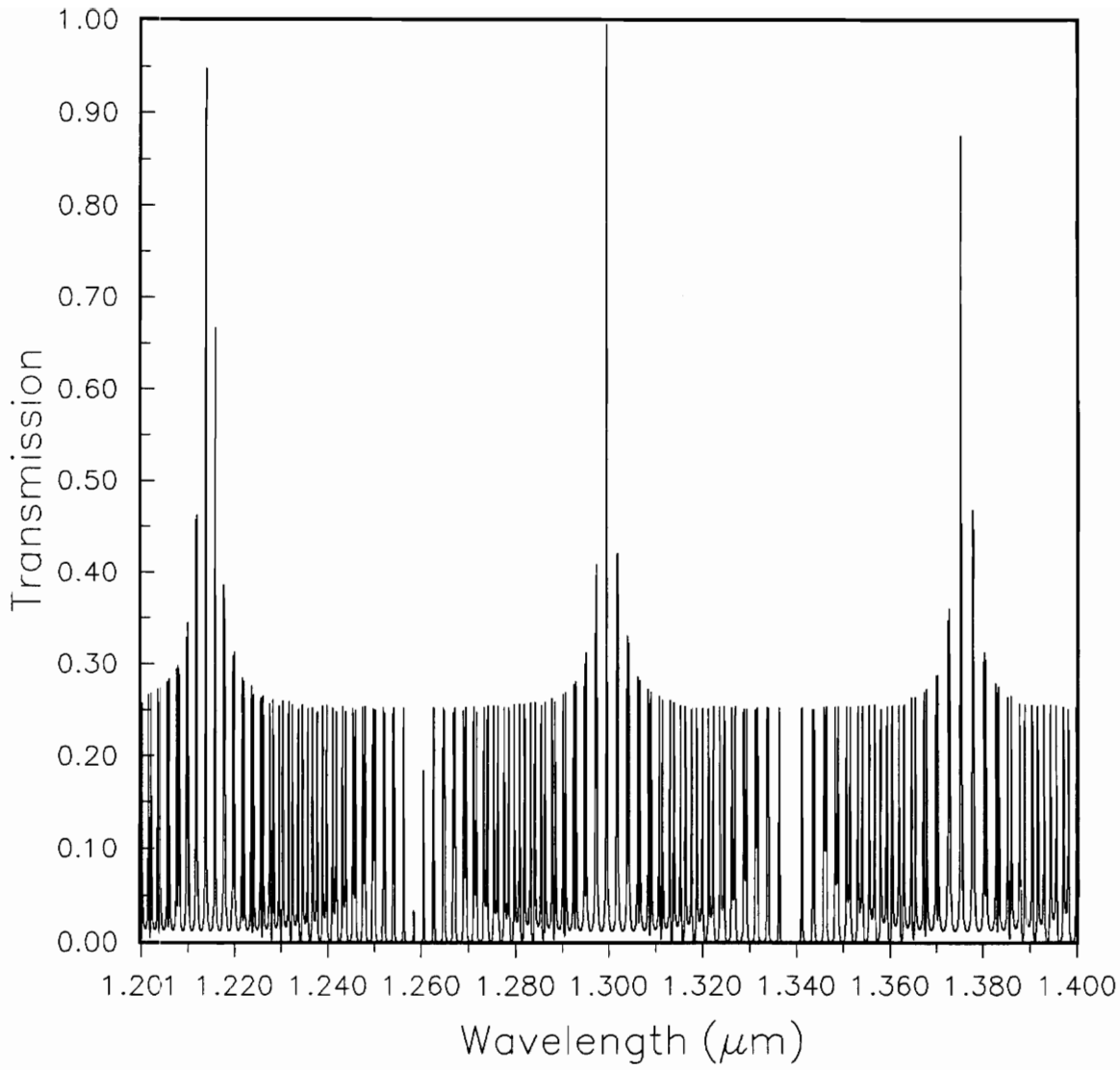

Figure 6.7: Spectral characteristic of cavity resonator of with peak transmission at 1300 nm. Parameters are $n_1 = 3.75$, $n_2 = 3.2$, $a = 0.08\ \mu m$, $d = 0.08\ \mu m$, $L = 99.71\ \mu m$ and $r = 0.9$.

Similar to the identical waveguide case, the main resonances can only occur at the peaks of $(k_{12}^2/s^2)\ \sin^2(sL)$ and the magnitudes of the main resonances are limited to the peak of $(k_{12}^2/s^2)\ \sin^2(sL)$. As wavelength moves away from the phase-matched point, the phase mismatch δ increases and the peak value of the envelope function $(k_{12}^2/s^2)\ \sin^2(sL)$ decreases. Theoretically, if the phase mismatch increases rapidly as wavelength deviates away from the phase-matched point (i.e., $d\delta/d\lambda$ is large), the other main resonances except the one nearest the phase-matched point can be eliminated. In such a case, there is only one peak transmission in the whole spectrum and thus the tuning range is arbitrarily increased.

Figure 6.8 shows the transmission characteristic of a coupled-waveguide F-P resonators with nonidentical guides. It is seen that the response is slightly better than that of identical waveguide case. The reason is $d\delta/d\lambda$ of the two guides and thus the phase mismatch effect is small. Figure 6.9 shows the characteristic curves of the two guides. Large $d\delta/d\lambda$ means large intersection angle at the phase-matched points. Because TE_0 modes of the two guides both have zero cutoff frequency, the intersection angle is limited to small values. To remove this difficulty, the index profile of one guide should be altered so that the first TE mode exhibits a non-zero cutoff frequency. This may be achieved by making one guide an asymmetrical one. Since this thesis is primarily aimed at exploring basic properties of coupled-waveguide Fabry-Perot resonators/filters, the extension to asymmetrical guides is suggested for future work.

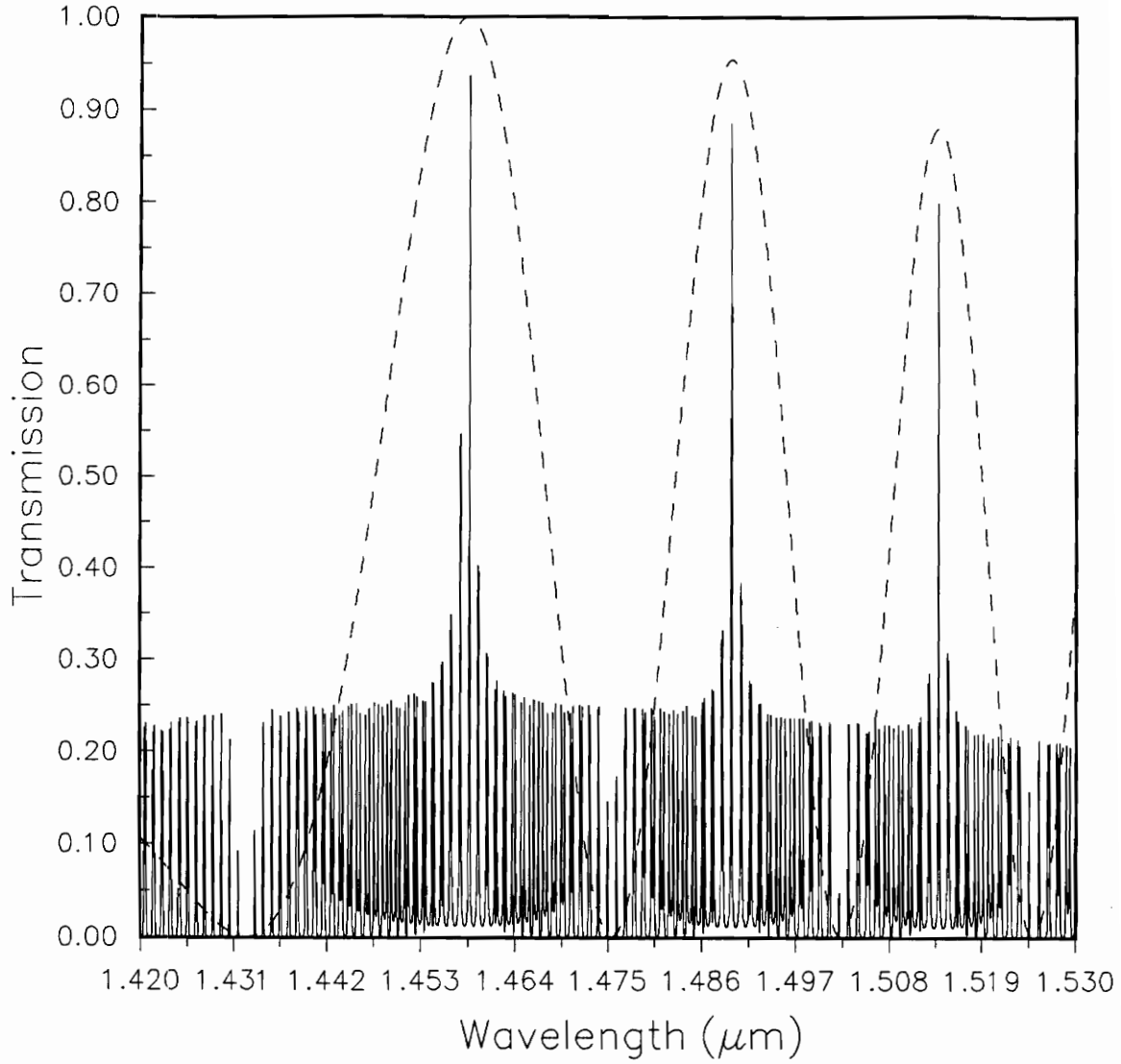

Figure 6.8: Transmittance spectrum of a nonidentical-waveguide F-P resonator with parameters $n_1 = 3.56$, $n_2 = 3.0$, $n_3 = 1.45$, $a_1 = 0.1\ \mu m$, $a_2 = 0.4\ \mu m$, $d = 0.1\ \mu m$, $L = 303.55\ \mu m$ and $r = 0.9$.

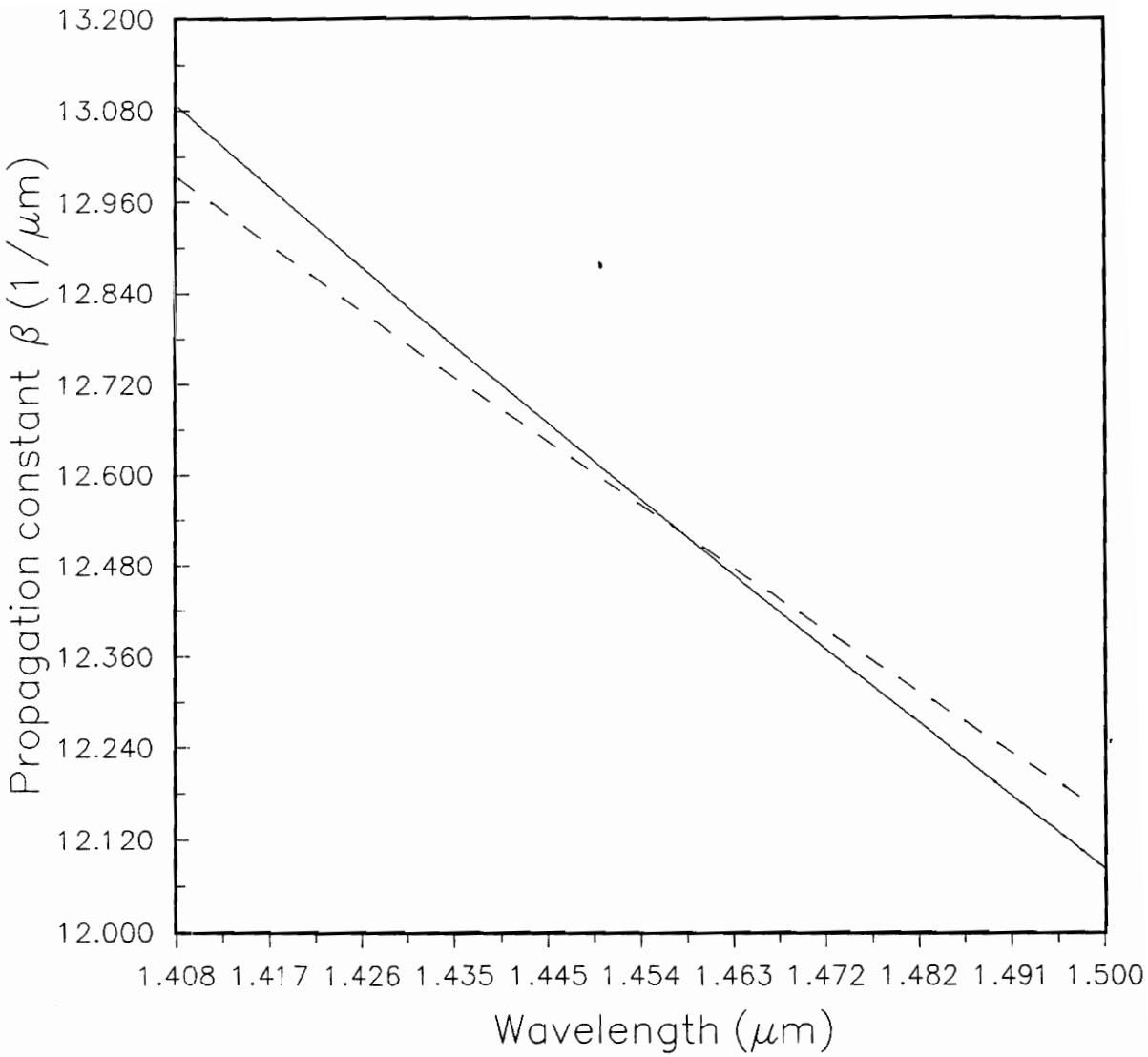

Figure 6.9: Dispersion characteristic curves of two nonidentical guides. Parameters of the two guides are $n_1 = 3.56$, $n_2 = 3.0$, $n_3 = 1.45$, $a_1 = 0.1\ \mu m$, $a_2 = 0.4\ \mu m$.

Chapter 7

Conclusion

7.1 Conclusions

A novel coupled-waveguide Fabry-Perot structure has been proposed and studied using coupled-mode theory. This structure exhibits the characteristic features of both Fabry-Perot resonator and directional coupler. The proposed device offers advantages over the conventional F-P resonator. It has a better mode discrimination capability (increased longitudinal mode spacing) than the single cavity F-P resonator because of the presence of a second guide as an external feedback. Due to the optical feedback from the end mirrors, this device, as a filter, exhibits a much narrower spectral width than the directional coupler filter.

Spectral characteristics of the proposed coupled-waveguide F-P structure were calculated using a coupled-mode theory based on the mode partition approach. Two geometries, namely identical-waveguide and nonidentical-waveguide structures were examined. The major advantage of the nonidentical-waveguide structure is the phase mismatch between the two guides and thus non-periodic resonance/transmission characteristics. Numerical results for several example cases were presented. For these

cases, the $-3\ dB$ spectral width is less than $0.1\ nm$ and the sidelobe level is $-3.8\ dB$ at $1.3\ \mu m$ and $-4.8\ dB$ at $1.55\ \mu m$. The influence of parameter variations on spectral properties were also examined. Larger coupling coefficient results in smaller immediate neighboring sidemode level but also a smaller mode spacing between main resonances. Coupling coefficient is decreased with increasing the separation between the two guides. Adjustment of the cavity length can be used to shift the main resonance to a desired wavelength.

Although the performance of the proposed resonator is not comparable to that of distributed-feedback structures, it is a simpler structure and thus is much easier to fabricate. The performance of the device can be improved considerably by cascading two or more such devices just as in multiple cavity F-P resonators. However, adding another cavity causes alignment problems and more scattering loss through the mirrors.

7.2 Suggestions for Future Work

For the identical-waveguide structure, the mode discrimination capability is achieved solely from the mode coupling effect. In the nonidentical waveguide structure , in addition to mode coupling, the phase mismatch can also be utilized to enhance the wavelength selectivity of the device. For this feature to be effectively exploited, the rate of change of phase mismatch has to be large, which means a larger intersection angle between the two dispersion characteristic curves at the phase-matched wavelength.

If one of the two guides is asymmetrical its fundamental mode has a non-zero cutoff frequency, and the intersection angle between the characteristic curves is expected to

be large. Another possibility is the adoption of a W-index profile for one waveguide. It has been shown [30] that waveguides with W-index profiles might exhibit a nonzero cutoff for the fundamental mode and hence provide a larger intersection angle than those with simple step-index profiles. Finding the waveguide parameters whose characteristic curves have a large angle at a desired phase-matched point will be a major task for future research. Furthermore, it is necessary that the main resonances occur at the phase-matched point. This requires a systematic search and implementation of some optimization technique.

Another suggestion for improving the results of this work is to extend the two-waveguide structure to a multiguide structure. Adding one or more parallel waveguides amounts, in effect, to further restricting the resonance condition and thus enhancing the mode discrimination capability of the device. For all-fiber spectral filters, it has been shown that triple-core fibers improve the sidelobe level over the dual-core fibers in square power [19]. In the case of planar waveguides, it is expected that the multiguide structure should offer the same improvement for sidelobes.

References

[1] G. P. Agrawal and N. K. Dutta, *Long-Wavelength Semiconductor Lasers*, Van Nostrand Reinhold, New York, 1986, ch. 7.

[2] J. R. Pierce, "Coupling of Modes of Propagation," J. of Applied Physics, vol. 25, pp.179-183, 1954.

[3] A. Yariv, "Coupled-Mode Theory for Guided-Wave Optics," IEEE j. Quantum Electron., vol. QE-9, pp. 919-933, 1973.

[4] H. F. Taylor and A. Yariv, "Guided Wave Optics," Proc. IEEE, vol. 62, pp. 1044-1060, 1974.

[5] A. Yariv, *Optical Electronics*, Holt, Rinehart and Winston, New York, 4th ed., 1991, ch. 13.

[6] D. Marcuse, *Theory of Dielectric Optical Waveguides*, Academic Press, San Diego, 2nd ed., 1991.

[7] D. Marcuse, *Light Transmission Optics*, Van Nostrand, New York, 2nd ed., 1982.

[8] H. Kogelnik, "Theory of Dielectric Waveguides" in *Integrated Optics*, T. Tamir Ed., Springer-Verlag, New York, 1975, ch. 2.

[9] A. W. Snyder, "Coupled-Mode Theory for Optical Fibers," J. Opt. Soc. Amer., vol. 62, pp. 1267-1277,1972.

[10] P. D. McIntyre and A. W. Snyder, "Power Transfer between Optical Fibers," J. Opt. Amer., vol. 63, pp. 1518-1527, 1973.

[11] H. A. Haus, W. P. Huang, S. Kawakami, and N. A.Whitaker, "Coupled-Mode Theory of Optical Waveguides," J. Lightwave Technol., vol. LT-5, no. 1, pp. 16-23, 1987.

[12] A. Hardy and W. Streifer, "Coupled Mode Theory of Parallel Waveguides," J. Lightwave Technol., vol. LT-3, pp. 1135-1146, 1985.

[13] H. C. Chang, "Coupled-Mode Equations for Dielectric Waveguides Based on Projection and Partition Modal Amplitudes," IEEE J. Quantum Electron., vol. QE-23, No. 11, pp. 1929-1937, 1987.

[14] S. L. Chuang, "A Coupled-Mode Formulation by Reciprocity and a Variational Principle," J. Lightwave Technol., vol. LT-5, pp. 5-15, 1987.

[15] E. Marcatili, "Improved Coupled-Mode Equations for Dielectric Guides," IEEE J. Quantum Electron., vol. QE-22, pp. 988-993, 1986.

[16] H. Nishihara, M. Haruna and T. Suhara, *Optical Integrated Circuits*, McGraw-Hill, New York, 1989, ch. 10.

[17] H. Kogelnik and R. V. Schmidt, "Switched Directional Couplers with Alternating $\Delta\beta$," IEEE J. Quantum Electron., vol. QE-12, pp. 396-401, 1976.

[18] G. A. Bogert, E. J. Murphy and R. T. Ku, "Low Crosstalk 4×4 $Ti : LiNbO_3$ Optical Switch With Permanently Attached Polarization Maintaining Fiber Array," J. Lightwave Technol. vol. LT-4, pp. 1542-1545, 1986.

[19] A. Safaai-Jazi and J. C. McKeeman, "All-Fiber Spectral Filter With Nonperiodic Bandpass Characteristics and High Extinction Ratio in the Wavelength Range $0.8\ \mu m < \lambda < 1.6\ \mu m$," J. Lightwave Technol., vol. LT-9, No. 8, 1991.

[20] R. C. Alferness and R. V. Schmidt, "Tunable Optical Waveguide Directional Coupler Fiber," Appl. Phys. Lett., vol. 33, pp. 161-163, 1978.

[21] Y. Sakakibara et al, "Single-Mode Oscillation under High Speed Direct Modulation in GaInAsP/InP Integrated Twin-Guide Laser with Distributed Bragg Reflector," Electron. Lett., vol. 16, pp. 456-458, 1980.

[22] R. C. Alferness and P. S. Cross, "Filter Characteristics of Codirectionally Coupled Waveguides with Weighted Coupling," IEEE J. Quantum Electron.,vol. QE-14, pp. 843-847, 1978.

[23] R. Zengerle and O. G. Leminger, "Narrowband Wavelength-Selective Directional Couplers made of Dissimilar Single-Mode Fibers," J. Lightwave Technol., vol. LT-5, No. 9, pp. 1196-1198, 1987.

[24] W. B. Jones, *Introduction to Optical Fiber Communication System*, Holt, Rinehart and Winston, New York, 1988, ch. 6.

[25] B. A. Saleh and M. C. Teich, *Fundamentals of Photonics*, Wiley, New York, 1991, ch. 9.

[26] J.Stone and D. Marcuse, "Ultrahigh Finesse Fiber Fabry-Perot Interferometers," J. Lightwave Technol., vol. LT-4, No. 4, pp.382-385, 1986.

[27] A. A. M. Saleh and J. Stone, "Two-Stage Fabry-Perot Filters as Demultiplexers in Optical FDMA LAN"s," J. Lightwave Technol., vol. LT-7, No. 2, pp. 323-330, 1989.

[28] H. van de Stadt and J. M. Muller, "Multimirror Fabry-Perot Interferometers," J. Opt. Soc. Amer., vol. 12, No. 8, pp. 1363-1370, 1985.

[29] D. Lee, *Electromagnetic Principles of Integrated Optics*, Wiley, New York, 1986, ch. 4.

[30] C. J. Chung and A. Safaai-Jazi, "Narrow-Band Spectral Filter Made of W-Index and Step-Index Fibers," J. of Lightwave Technol., vol. LT-10, No. 1, pp. 42-45, 1992.

Vita

Cheng-Chun Chang was born in Tamsui, Taiwan, Republic of China in 1963. He finished his college education at National Taiwan University in 1985. After receiving the B. S. degree in Civil Engineering, he served the army of the Republic of China from 1985 to 1987.

He entered the Department of Engineering Science and Mechanics at Virginia Tech in 1988 and received an M. S. degree in 1990. He then joined the Electrical Engineering Department of Virginia Tech as an M. S. student. After receiving the M. S. degree in Electrical Engineering, he plans to pursue a Ph. D. degree in Electrical Engineering.